Cone model-based SEP event calculations for applications to multipoint observations

J.G. Luhmann [a,*], S.A. Ledvina [a], D. Odstrcil [b], M.J. Owens [c], X.-P. Zhao [d], Yang Liu [d], Pete Riley [e]

[a] Space Sciences Laboratory, University of California, 7 Gauss Way, Berkeley, CA 94720, USA
[b] University of Colorado, CIRES-NOAA/SEC, 325 Broadway, Boulder, CO 80305, USA
[c] Center for Space Physics, Boston University, 725 Commonwealth Ave, Boston, MA 02215, USA
[d] W. W. Hansen Experimental Physics Laboratory, Stanford University, Stanford, CA 94305, USA
[e] Science Application International Corporation, San Diego, CA 92121, USA

Abstract

The problem of modeling solar energetic particle (SEP) events is important to both space weather research and forecasting, and yet it has seen relatively little progress. Most important SEP events are associated with coronal mass ejections (CMEs) that drive coronal and interplanetary shocks. These shocks can continuously produce accelerated particles from the ambient medium to well beyond 1 AU. This paper describes an effort to model real SEP events using a Center for Integrated Space weather Modeling (CISM) MHD solar wind simulation including a cone model of CMEs to initiate the related shocks. In addition to providing observation-inspired shock geometry and characteristics, this MHD simulation describes the time-dependent observer field line connections to the shock source. As a first approximation, we assume a shock jump-parameterized source strength and spectrum, and that scatter-free transport occurs outside of the shock source, thus emphasizing the role the shock evolution plays in determining the modeled SEP event profile. Three halo CME events on May 12, 1997, November 4, 1997 and December 13, 2006 are used to test the modeling approach. While challenges arise in the identification and characterization of the shocks in the MHD model results, this approach illustrates the importance to SEP event modeling of globally simulating the underlying heliospheric event. The results also suggest the potential utility of such a model for forcasting and for interpretation of separated multipoint measurements such as those expected from the STEREO mission.
Published by Elsevier Ltd. on behalf of COSPAR.

Keywords: Solar energetic particle events; Shock acceleration of particles; Space weather

1. Introduction

Several decades of solar energetic particle (SEP) event observations have led to important conceptual pictures of the relationships between the ion flux time profiles and their associated solar and interplanetary events (Cane et al., 1988; Reames, 1999; Tylka, 2001; Klecker et al., 2006). The great majority of SEP ions are protons which reach energies up to the GeV range on occasion. Significant events involve a moving, evolving shock source that may survive well past 1 AU. These SEP events are often referred to as gradual events due to their long duration (up to several days) compared to the smaller impulsive events commonly associated with small-to-modest flares. Gradual events observed at the Lagrangian upstream location (L1) typically start around the time of a Coronal Mass Ejection (CME) that is headed toward Earth, and therefore appears as a 'halo' around the solar disk in coronagraph images (e.g. Kahler, 2007). Radio bursts accompanying these CMEs are thought to signify the early formation of a shock wave that evolves as the coronal plasma and magnetic field making up the CME ejecta moves outward and expands.

* Corresponding author.
  E-mail address: jgluhman@ssl.berkeley.edu (J.G. Luhmann).

The first SEP particles may arrive when the shock is still close to the Sun, at which time the observer may see a beamed or anisotropic distribution of particles focused along the interplanetary magnetic field (e.g. Reames et al., 2001). The highest energies arrive first, as the fastest particles emitted by the early shock win the race to reach the observer. Interplanetary shocks produced by CMEs have been inferred to either accelerate and then decelerate in the case of modest CME velocities ($\sim$<600 km/s), or to decelerate continuously for CMEs that start with very high speeds (up to $\sim$2500 km/s) close to the Sun. If the shock crosses the 1 AU observer's location, the beamlike nature of the SEP pitch angle distribution broadens and the flux at lower (< a few MeV) energies may be enhanced as if these particles are temporarily trapped in its vicinity. This so-called ESP or Energetic Storm Particles event is a special part of gradual SEP events that provides a look inside the shock source itself. The CME ejecta may also be detected in the post-shock plasma and magnetic field data, and is often associated with a reduction in the SEP event intensity, as if its magnetic fields form a barrier to their entry into that structure (e.g. Cane, 2000). The complete in-situ structure of shock and ejecta, usually referred to as an ICME or Interplanetary CME, thus provides important complementary information when interpreting a measured SEP event profile.

Theoretical work related to the acceleration and transport of shock-generated SEPs has similarly developed over decades (e.g. Lee, 1983, 2005; Ng and Reames, 1994; Giacalone and Kota, 2006). The generally held paradigm involves diffusive acceleration and scattering by waves, both ambient and self-generated, as primary factors in describing what is observed (e.g. as treated analytically by Lee, 2005). Various assumptions, usually involving the solution of some form of Boltzmann equation in a spherical geometry, have been introduced to obtain both analytical and numerical descriptions of gradual SEP event time profiles, including ion composition variations (e.g. Ng and Reames, 1994; Ng et al., 1999). In particular, these theoretical treatments suggest the extent to which the particles can be viewed as moving through a prescribed background magnetic field, with scattering from ambient field fluctuations, versus generating their own scattering centers through anisotropy-related instabilities (e.g. see the discussion by Tylka, 2001). However, the ability to include realistic background coronal and solar wind structure, and to simulate real events that consistently combine the ICME and SEP events, has remained elusive.

Realistic SEP event models are a highly desired part of space weather simulations, due to both their fundamental interest as an astrophysical research tool and the practical need for related hazard predictions (e.g. Balch, 1999; Mewaldt, 2006). A successful SEP event model relies on the successful description of the background heliospheric plasma and magnetic field, both ambient and disturbed, as well as the SEP source(s) and transport. Compounding these challenges, SEP sources include both flare and CME/ICME shock contributions, with a possible role for background suprathermal ion seed populations (e.g. Cane et al., 2003). In spite of these difficulties, a few attempts have been made to numerically model the shock-accelerated component of SEP time profiles, both semi-empirically (see Heras et al., 1992; Kallenrode and Wibberenz, 1997; Lario et al., 1998; Aran et al., 2006, 2007, 2008) and using MHD models of an interplanetary shock together with the assumption of diffusive acceleration and transport (Li et al., 2003; Kota et al., 2005; Kocharov et al., 2009). All of these methods rely on various simplifying assumptions to either make the problem more mathematically or computationally tractable, or to fill in for poorly constrained parameters. These include adopted descriptions of the scattering magnetic field fluctuations and/or diffusion coefficients, and of the underlying large scale plasma and magnetic field geometry including the moving shock. In general, the issue of how much of a gradual SEP event time profile is determined by the evolving shock properties and observer connection details, versus the diffusive aspects of shock acceleration and particle transport, is rarely emphasized and not yet resolved. Diffusive processes, or their 'focused diffusion' variants (e.g. Ruffolo et al., 1998), are generally presumed to dominate. Yet the shock source evolution is an essential factor in the physics of the problem and in defining real event profiles (e.g. see Heras et al., 1992, 1994; Kallenrode and Wibberenz, 1997).

The approach described by Luhmann et al. (2007), for $\sim$10–100 MeV protons, provides another alternative that emphasizes and tests for the shock evolution importance in SEP event profiles. In this case both the shock and SEP transport information are derived from an MHD model of an ICME that is initiated using a cone model description of a CME derived from coronagraph images (Howard et al., 1982; Fisher and Munro, 1984; Zhao et al., 2002). The realistic ambient solar wind MHD simulation is based on photospheric magnetograms, while the ICMEs are created by the cone model-based injection(s) of high speed, high density 'gusts' at the inner boundary of the solar wind model (Odstrcil et al., 2004, 2005). We use a particular version of this combined CME cone model and MHD solar wind model called CORHEL, developed and tested as part of the Sun-to-Earth space weather simulation of the Center for Integrated Space Weather Modeling – CISM (Luhmann et al., 2004). This simplified approach to ICME modeling provides a first-order 3D, time-dependent description of an interplanetary shock and the interplanetary conditions resulting from a particular observed CME, similar to the earlier models of Dryer (1996) and Fry et al. (2003) (also see Smith et al., 2009). Our method then treats the SEP source as a shock strength-parameterized 'black box', similar to the semiempirical models of Heras, Kallenrode, Lario and their coauthors. The SEP protons are injected onto a sequence of the observer-connected model field lines intersecting the moving shock location, after which they adiabatically propa-

gate in the ambient modeled magnetic fields without further scattering to an observer at 1 AU. Significant differences from others' earlier models, in addition to the nominally scatter-free transport assumption, include the ways in which the time-dependent 3D MHD simulation results are incorporated (as described below). Here the results from three CORHEL case studies are used to demonstrate the extent to which the simplest form of the model approximates the related observed proton events, including one detected by the STEREO spacecraft.

In the following sections, the CORHEL results for the well-studied May 12, 1997 CME case, previously treated in Luhmann et al. (2007), and two other halo CME events in November, 1997 and in December 2006 soon after the STEREO (Solar Terrestrial Relations Observatory) launch, are first described. These events were selected because they had fairly simple, readily identified SEP events and because their cone model parameters had previously undergone some testing in order to produce reasonable descriptions of L1 point observations surrounding their related ICME passage. The May 1997 case used here is based on a newer cone model parameter set and shock identification procedure than were used in the Luhmann et al. (2007) initial SEP event model test. In addition to presenting additional examples of our scheme for L1 SEP events, we compute SEP event profiles for a number of other 1 AU locations with respect to the Earth. These illustrate the longitudinal dependence of the modeled events, including the potential for applications to STEREO multipoint measurement interpretation as the spacecraft continue to separate. We note this model has been designed to run without user intervention once a set of CME cone model parameters has been determined from coronagraph observations of a CME. It is thus potentially suited to a forecast mode of operation, although a SEP event may well be in progress already by the time the cone model parameters have been derived.

2. Assumptions of the SEP event model

As noted above, and described in Luhmann et al. (2007), our approach to SEP event modeling differs from others, including that of Kocharov et al. (2009) who also uses a combined CME cone/solar wind model, and Aran et al. (2007, 2008) who use a similar solar observation-based MHD ICME model. Although these other authors similarly incorporate information on the shock derived from the MHD simulation results, our baseline assumption is that the influence of the shock evolution dominates over diffusive transport in determining the SEP time profiles. In the present version of our model, previously run CORHEL results are first analyzed by a shock identification algorithm (described below) that both locates and characterizes the simulated ICME shock on observer-connected field lines in snapshots of the gridded MHD variables. A SEP event is then simulated with a series of impulsive particle injections from the location of the ICME shock on the

sequence of observer-connected field lines. No a priori assumption is made about near-Sun injection (e.g. Kocharov et al., 2009), or that knowledge can be derived from the measured SEP event to describe the time-dependent shock injections (e.g. Aran et al., 2007). The present model is a completely forward-modeling approach with the exception of the magnetograph-derived solar wind boundary conditions, and coronagraph-derived cone parameters that characterize the ICME in the CORHEL code. For each field line the injected flux and energy spectrum depend on the shock properties and occur at the time of observer connection only. The results of these impulsive injections are then integrated to approximate what is observed, in a Green's function manner (also see Kallenrode and Wibberenz, 1997, for use of a similar philosophy of SEP event reconstruction). This is a simplifying approximation based on the additional assumption that the particles generated around the time of the observer connection dominate what is detected.

We note that if unlimited access to a supercomputer was assumed, one could take the more accurate first steps of determining the entire SEP time profile on every field line in the model that the observer is ever connected to throughout the event. This would entail first determining the observer-connected field lines for every CORHEL code time step, and then tracing them back to their solar latitude and longitude of origin. One would then have to recover the complete history of the field line rooted at that location on the Sun (assuming no field line footpoint movement) for all earlier time steps, including the shock history on it (not just the shock parameters at the time of observer connection as is done in our current approach). Next the entire time profile of the SEPs on each field line that the observer is ever connected to would need to be computed. Finally, the 'observer event profile' would be constructed from the sequence of individual field line SEP profiles by adopting the flux and spectrum at the time of observer connection for each field line. This concept was illustrated in Luhmann et al. (2007, JASR v.40, in Fig. 4, right column). Hence one of the purposes of the present case studies is to test the simplifying assumption that the contribution to a SEP event from each observer-connected field line is dominated by the flux and spectrum injected at the time of observer connection to the shock.

Here we also invoke the simplest scenario, neglecting any special treatment related to the ESP (Energetic Storm Particle) increases of particle flux associated with the shock passage, any contributions of related or ongoing flares at the Sun or any prior CME activity, and any dependence of the shock source injection on the shock normal angle. The injected 10–100 MeV protons have an isotropic angular distribution, with a power law energy spectrum and intensity dependent on the shock jumps from the CORHEL model results. In the present model we adopt a spectral index often used to describe the results of diffusive acceleration within the shock vicinity, depending on the compression ratio dn according to the formula $(dn + 2)/$

$(dn - 1)$ (e.g. see Jones and Ellison, 1991). The intensity of each injection Q is weighted by a velocity jump (dV)-dependent factor according to $\log Q \sim dV$ as empirically derived in earlier models (see Lario et al., 1997). An additional $1/r^2$ factor allows for the dilution of flux due to radial expansion with distance from the Sun. Further numerical experimentation with this source description, including provision for evolving spectral shapes, is planned. As previously noted we further assume that all energization occurs at the injection site at the shock.

The subsequent transport in the CORHEL interplanetary fields is scatter-free, but includes any mirroring dictated by the field topology along the particle trajectories. Again, a primary aim of these calculations is to test our assumptions about the dominant factor(s) defining shock-related SEP event profiles, which are in contrast to other treatments emphasizing diffusive acceleration and transport throughout the inner heliosphere at the outset. While we have reduced the problem to its most elementary level to start, the scheme allows the option to add in Monte-Carlo-like pitch angle scattering during transport (e.g. Scholer and Morfill, 1975), or other approximations that mimic diffusive effects (e.g. Pei et al., 2006) as comparisons with observations demand. It is also relatively straightforward to add fixed flare sources at the inner boundary. Testing these additions is beyond the scope of the present study, which is designed to investigate how much influence the moving shock source profile and interplanetary field configuration have on their own.

There are a number of additional questions that can be explored within this model framework. For example, it is a straightforward matter to add shock normal angle as a parameter in characterizing the intensity and spectrum of the injections at the shock (e.g. Tylka and Lee (2006) discuss a possible shock normal angle effect on the shock source although Lario et al. (1998) found no clear empirical evidence in the sample of events they analyzed). Event anisotropy histories are another property that contains important information, in this case regarding the importance of scattering in SEP acceleration and propagation (e.g. Reames et al., 2001). Anisotropies in the scatter-free version of the SEP event model are determined only by the combination of any specified anisotropies at the source (none assumed here) and the magnetic focusing or mirroring forces on the particles along their paths to the observer. The model automatically produces a focused distribution early in the event when the observer is connected to the shock source close to the Sun, and an isotropic distribution when the shock arrives at the observer. However we defer discussion of the anisotropy evolution to a subsequent report with usable multipoint anisotropy data, e.g. from STEREO spacecraft observations.

In fact the most important addition needed for the next model versions is arguably inclusion of the coronal portion of the ICME shock (inside 20–30 solar radii, Rs), which is currently not part of CORHEL or any of its cone model-using counterparts. Although all parts of the inner heliosphere shock and field provided to the SEP model codes

are automatically included in the SEP event calculation, CORHEL models with detailed CME descriptions in the coronal portion of the model, while in the process of development, are not yet available. In addition to testing how well our approach can work without the coronal shock, the version used here may be particularly applicable to SEP events from slower (<600 km/s) CMEs, whose shocks typically form or strengthen at the greater heliospheric distances within the ENLIL domain ($r > 20$ Rs). Because we generally lack in-situ measurements along the path of the shock from the Sun to the observer at 1 AU, good agreement of the CORHEL cone model results with L1 plasma and field observations, at least in shock time-of-arrival and shock strength, provides some confidence that the ICME propagation is adequately described by the MHD simulation.

3. Cone model-initiated disturbances in the solar wind

The cone model of CMEs was originally created to provide generalized 3D geometrical descriptions of the structure of CMEs seen in coronagraph images (Howard et al., 1982). Zhao et al. (2002) adopted this model for Solar and Heliospheric Observatory (SOHO) images, developing systems of parameters and assumptions for routine application. Cone model parameters provide information on the size, speed, location and direction of the injected CME material, under the assumption that the 3D cone whose axis defines the ejecta direction has a circular base cross-section. (We note that recently Zhao (personal communication, 2008) developed a new model with an elliptical cone base.). Odstrcil et al. (2004, 2005) integrated the option for cone model injections of high speed and density 'gusts' into his ENLIL MHD solar wind model to mimic ICMEs and their effects. Because cone model injections lack ejecta magnetic fields, they produce interplanetary disturbances most representative of the shock and sheath portion of an ICME.

Both CORHEL and other similar models available at CCMC (Community Coordinated Modeling Center) provide user-oriented versions of the combined cone model/ ENLIL solar wind model. The CORHEL simulations of ICMEs use MAS MHD coronal model results (see Riley et al., 2001) for the inner boundary conditions for the ENLIL ambient solar wind at ∼20–30 Rs (solar radii) (e.g. Luhmann et al., 2004). The modeled solar wind produced by CORHEL has been extensively evaluated by Owens et al. (2008), who find that it generally captures the large scale solar wind stream structures, features important to accurately model both ICME propagation and the connectivity of an observer to the shock along field lines. Cone model parameters from coronagraph image fits used in the CORHEL model are generally derived by the Stanford group, and in some cases have been adjusted by trial-and-error experimentation to achieve the best fit to L1 in-situ signatures of the ICME.

Previous reports (e.g. Odstrcil et al., 2004, 2005) have described the details of the interplanetary disturbances pro-

duced by launching cone models within CORHEL. The ambient solar wind conditions are established by running CORHEL until a quasi-steady state is achieved. This ambient wind may be a nearly dipolar solar wind near solar minimum, but most often contains a moderate amount of stream structure dictated by the higher order multipolar contributions to the prevailing photospheric magnetic field (e.g. see Lee et al., 2009) for a description of the solar wind structure obtained with this model over an extended period). The cone model parameters are used both to locate the injection of the high density, high speed pressure pulse approximating the CME material, and to set its size, direction and speed of (radial) injection into the ENLIL solar wind model domain. The spherical cone front is adopted because it best represents the shape of the imaged coronal ejecta. Densities in the injected material are generally taken to be 4× the ambient density at the inner boundary of ENLIL. The result is a localized high pressure gust or wave that sweeps through ENLIL up to the CORHEL outer boundary of ∼2 AU heliocentric distance. This pressure wave is distorted by its interaction with the ambient solar wind structure and may steepen into a shock wherever its speed exceeds the local magnetosonic velocity, which varies with radius as well as with the solar wind structure. The interaction with the ambient wind may result in a lenticular concave cross-section if the injection is centered on the slow wind belt of the resulting solar wind (e.g. Riley et al., 1997). However it often produces a much more fragmented and complex disturbance (Odstrcil and Pizzo, 1999), even from the simply shaped injection, as the coronal and interplanetary surroundings are frequently asymmetrical or complex.

With the possible exception of the ISPM and HAF models of Fry et al. (2003) and Smith et al. (2009), only the cone model has been applied to a large enough number of real CME events to provide a sense of its overall performance, e.g. in describing such variables as shock arrival time and shock strength (Taktakishvili et al., 2009). Several demonstrations of the CORHEL cone model option described by Case et al. (2008) tested the sensitivity of the resulting ICME propagation to background solar wind conditions, but most previous published reports on its use have focused on the widely-studied halo CME on May 12, 1997 (e.g. Thompson et al. and references therein; Arge et al., 2004; Odstrcil et al., 2004, 2005). In addition to a well-observed and characterized ICME measured by Wind spacecraft in-situ instruments, this case also included a classic gradual SEP event. The good fit of the May 12, 1997 CORHEL model results to the ICME and its surroundings made it an ideal candidate for developing and testing a consistent SEP event simulation (Luhmann et al., 2007). The expansion on that earlier study described here further exercises that approach.

4. CORHEL models for the selected events

Fig. 1a–c show the in-situ OMNI measurements for the three events in May and November 1997 and in May 2006

selected for testing our model. The OMNI data, available at the National Space Science Data Center (King and Papitashvilii, 1994) provide as uniform an L1 data set as possible for events spanning several mission lifetimes, including solar wind plasma parameters, magnetic fields, and energetic particles. The 1997 data are primarily from the Wind spacecraft, while later data are mainly from ACE. As mentioned above, CORHEL requires the specification of a magnetic synoptic map, which is usually for the Carrington rotation including the event, the eruption time and location on the Sun, a description of the cone width and axis orientation derived from coronagraph images, and the speed of the observed CME at ∼20 Rs (also estimated from the images). The cone model parameters used for the events in this study are given in Table 1.

4.1. May 1997 event

The widely studied May 12, 1997 halo CME and its consequences have undergone intensive analysis, thanks to the unprecedented set of observations by the ISTP spacecraft, including SOHO and Wind (e.g. see Thompson et al., 1998; Plunkett et al., 1998; Webb et al., 2000). The simplicity of the solar disk at the time of this event made it a nearly ideal case for detailed interpretations using models, although the involved active region was very small with a strong magnetic field (e.g. see Liu, 2004). This case was selected by CISM as the focus of its first realistic end-to-end event simulation. The simulated initiation of the CME in the MAS coronal MHD model has been described at a number of venues and is in preparation for publication by Linker and coworkers (personal communication, 2008). In the meantime, the cone model of this event was subjected to intensive testing by Odstrcil et al. (2004, 2005) and Arge et al. (2004), to the point where it is one of the best examples of a cone model application to an observed CME/ICME. We were thus able to apply the cone model results for the May 1997 SEP event modeling with considerable confidence in the underlying solar wind and ICME shock description.

The observations of the main L1 plasma parameters and magnetic field magnitude for this event from the OMNI data base are summarized in Fig. 1a. This ICME has most of the classical signatures. A sudden jump in magnetic field, density and velocity occurs at the preceding shock on day 135, followed by approximately 1 day of enhanced field and velocity, but low to normal density. The period following the shock where the plasma density, velocity and field increase is generally interpreted as the shock driver sheath, composed of compressed, plowed-up solar wind, while the following interval with low to normal density but continuing high field is considered to be the driver or ejecta. The field vectors (not shown) exhibit slow rotations suggesting the passage of a twisted field structure or flux rope.

The measured SEP event profile for this case in the bottom panel of Fig. 1a is a nearly ideal example of a gradual
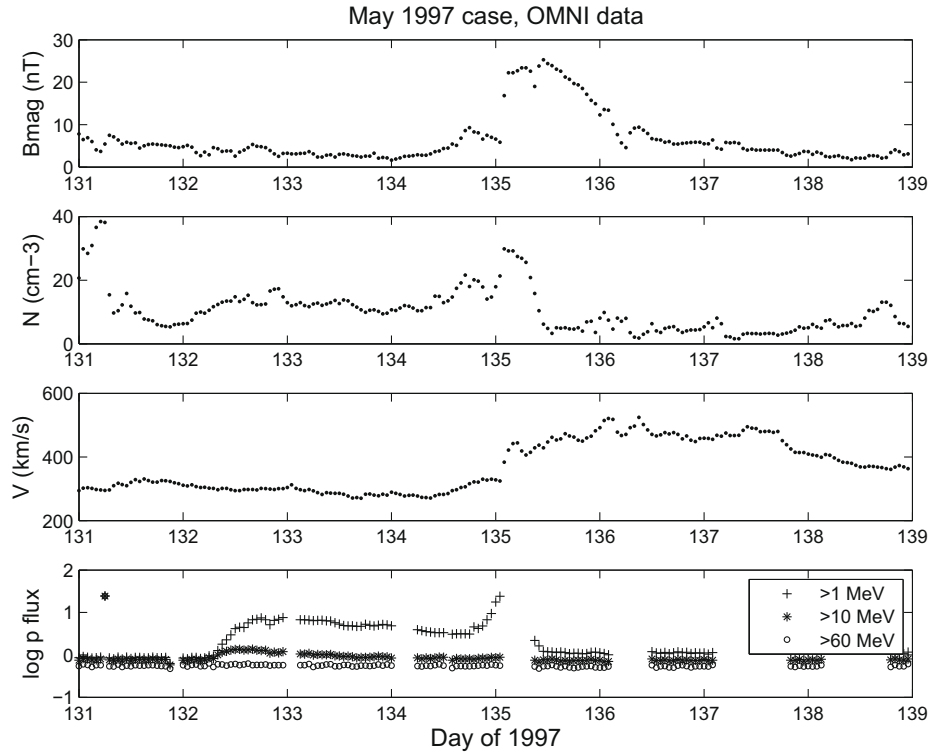
Fig. 1a. The ICME and SEP event at L1 from the May 12, 1997 Halo CME, as seen in the OMNI data. The top panel shows magnetic field magnitude (B_{mag}), followed in order by solar wind density (N), solar wind velocity (V) and log of the SEP event proton integral flux in the energy ranges shown in the legend.
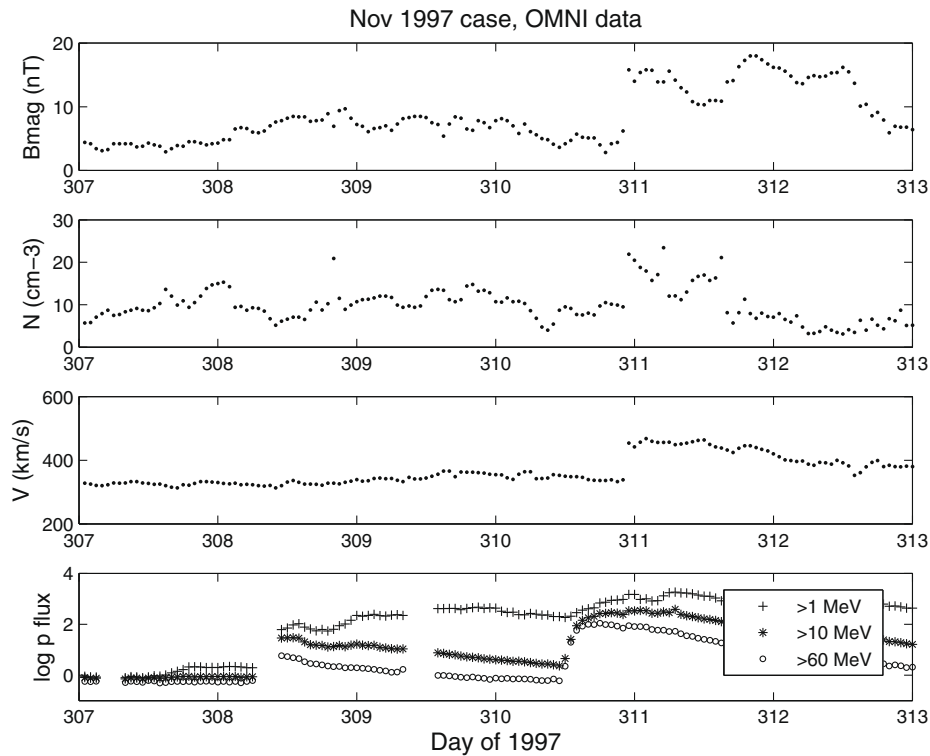

Fig. 1b. Same as Fig. 1a but for the November 4, 1997 halo CME. Note that a second CME and related ICME and SEP event occurred on November 6, but our current modeling does not include this second injection.
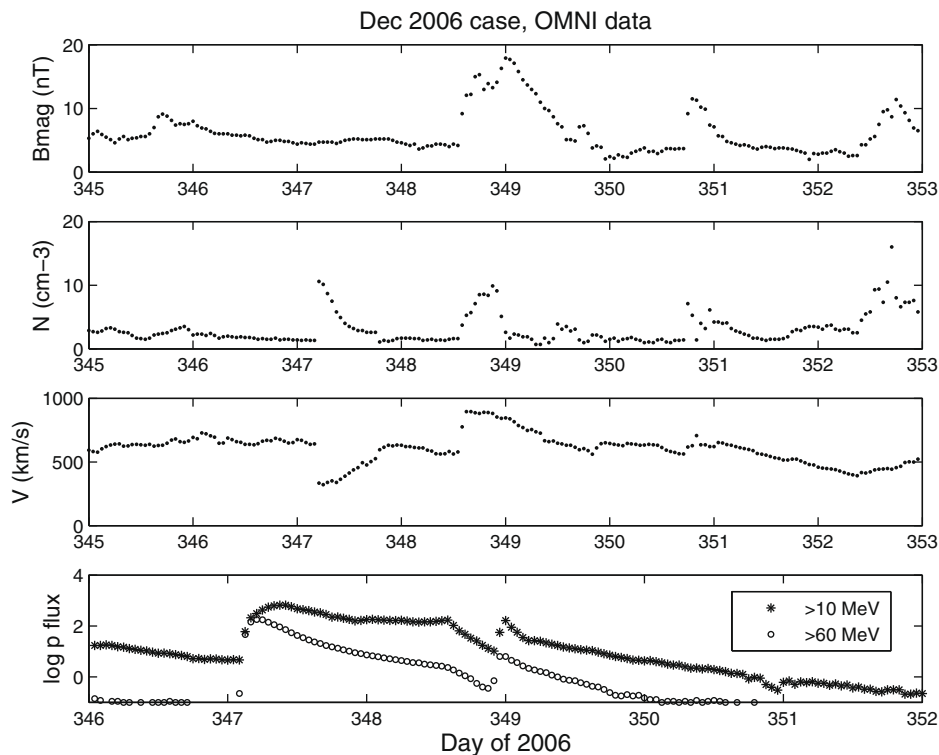
Fig. 1c. Same as Fig. 1a but for the December 13, 2006 halo CME. The lower energy data were not available in the OMNI data for this event.

Table 1
Description of the parameters used in the cone model CME initiations in CORHEL for the three cases studied.

Event	12 May 1997	4 Nov 1997	13 Dec 2006
Carrington rotation	1922	1929	2051
Cone info source	Odstrcil et al. (JGR, 2004)	Yang Liu fit	Xuepu fit
Cone eruption date	5/12/1997	11/4/1997	12/13/2006
Cone eruption time	16:47	13:16	03:53
Cone axis: angle from Solar North pole [°]	87	102	112
Cone axis: angle West from sub-Earth point [°][*]	181	185	196
Cone half-width [°]	25	65	56
Cone speed [km/s]	700	758	1217

[*] In CORHEL, the sub-Earth point defines the 180°. Longitude meridian to ensure the cone model CME injection is far from the edges of the synoptic map used for the solar boundary conditions. Edge effects are sometimes present in these maps.

event, with both a substantial prompt population arriving at L1 several days ahead of the ICME shock, and an ESP enhancement at the lowest energies at the time of shock arrival. It also shows some decrease following the shock arrival, presumably due to exclusion of the energetic particles by the CME ejecta or driver fields driving the ICME shock. The cone model does not include these ejecta fields and so we do not expect to be able to reproduce their influences on the modeled SEP profile. As in most previous SEP event modeling, success would be defined by capturing the pre-shock portion of the profile in this event.

The inner (20 Rs) boundary ambient solar wind velocity map used in the CORHEL model for this event, before the 700 km/s cone model-initiated CME injection, is shown in Fig. 2a. The CME location and cone model injection angular width at this radius is superposed on the conditions during Carrington Rotation (CR) 1922. As mentioned earlier,

in CORHEL the boundary conditions are derived from the MAS coronal MHD code results. The nearly central projected location of Earth relative to this simulated CME initiation footprint is marked by the small circle. The modeled ICME at the location of Earth is compared with the OMNI measurements in Fig. 2b. Fig. 2b also shows a snapshot of normalized solar wind density contours in the cone model in both ecliptic plane and meridional cross-sections (Earth is located inside the small white circle). Together, these illustrations give an idea of the state of the heliosphere during the injected material propagation, including the heliolatitudes of high and low speed solar wind, and the solar wind stream interaction compressions resulting from the non-uniform velocities at constant latitudes coupled with solar rotation.

From this first example it is easy to see why SEP event models that do not include underlying solar wind and
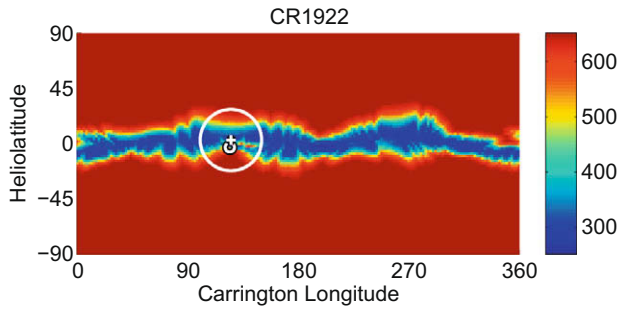
Fig. 2a. Inner boundary map for the solar wind portion of the May 12, 1997 CME event CORHEL model, showing color-coded solar wind velocity contours (color bar at right in km/s). This event occurred during Carrington Rotation (CR) 1929. The location and cross-section of the cone model CME injection for this case is indicated by the white circle. The relative location of the slow wind belt (blue), as well as its level of complexity, has significant influence over the way the cone model injection evolves between this boundary and 1 AU. (For interpretation of references to color in this figure legend, the reader is referred to the web version of this article.)

shock structure cannot be expected to produce realistic results. In particular, the low heliolatitude solar wind is so structured by its coronal source(s) that an assumption of a spherical shock that evolves self-similarly or symmet-

rically is highly unlikely. The lenticular shape of the post-shock compression, from the slow solar wind belt interaction of the ejection (Fig. 2a), is clearly seen in the meridional view in Fig. 2b. As the CME driver or ejecta fields are not modeled in this case, the lack of detailed agreement with the plasma and field observations in the post-shock disturbance, seen in the right panels of Fig. 2b, is expected. SEP fluxes usually decrease inside the ejecta in ecliptic plane events, suggesting their exclusion from the distinct topological structure of the ejecta. Our present model will not show this effect because of the modeled ICME limitations. However, what is most important for the SEP event modeling is the shock timing and strength history as represented by the jumps in the plasma parameters. Both the shock time of arrival at L1 and the shock strength as seen in the density compression are in general agreement with the OMNI data for this event. Furthermore, as previously discussed in Odstrcil et al. (2004, 2005) and Arge et al. (2004), the solar wind structure context of this event, determined by the CORHEL pre-injection solution for Carrington Rotation 1922, was also well-described by the model. If we use the L1 comparison as a measure of the likely success of the entire inner heliosphere simulation, this is the best example obtained.
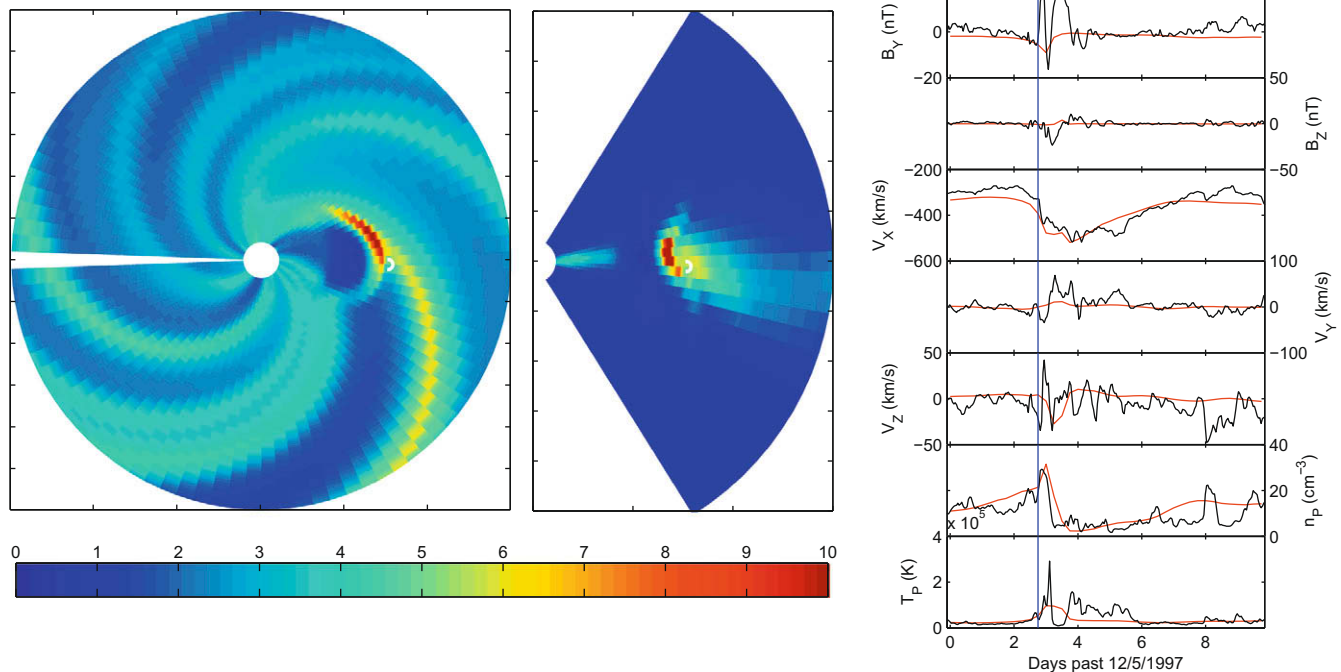

Fig. 2b. Snapshot of the simulation results at one time step (indicated by the vertical line on the time series of L1 data on the right), for the May 12, 1997 CORHEL model with the cone model CME. Earth's location is shown by the small white circle. The equatorial and meridional solar wind density perturbation contours are shown at left and center. (A background solar wind density profile falling off as the square of the heliocentric distance has been subtracted to emphasize the effects of the stream interactions and the CME-related disturbance.) The color bar indicates the contour levels in units of cm^{-3}. The cone model results for L1 are the red lines superposed on the in-situ data in black. In this time series the origin is the time of the cone model-determined CME 'injection' at the inner boundary of the solar wind part of the CORHEL model. (For interpretation of references to color in this figure legend, the reader is referred to the web version of this article.)
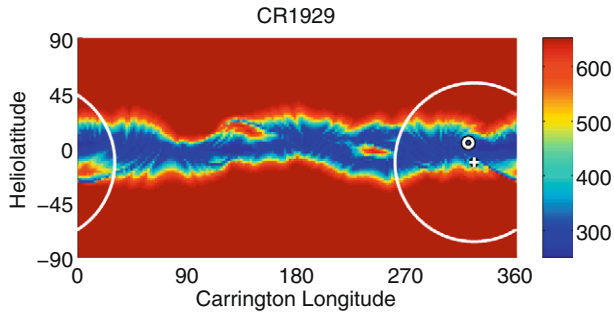
Fig. 3a. Same as Fig. 2a but for the November 4, 1997 CME.

4.2. November 1997 event

The November 4, 1997 halo CME was not as thoroughly analyzed as the May 1997 event, but it too benefited from the complementary coverage by SOHO imaging and Wind in-situ observations and was among the events studied in earlier observational papers (e.g. Mulligan et al., 1999; Mason et al., 1999; Eto et al., 2002). Mason et al. (1999) provide a description of the associated solar activity, which we will not repeat here. Fig. 1b displays the OMNI in-situ data, including the SEPs, for this event. This case was more complex at both the Sun and in the interplanetary medium. The November 4 CME was followed by a second significant CME on November 6 (associated with the same active region), that interacted with the earlier event's trailing portions. Type II radio bursts, indicating the formation of a shock in connection with the eruptions,

were observed for both events. The shock for the November 4 CME's ICME arrival occurs at the end of day 310, at a speed of ~470 km/s. Mulligan et al. (1999) show the details of the ICME magnetic field and discuss the different signatures observed at the WIND and NEAR spacecraft. It is not clear that either spacecraft observed the second ICME from the November 6 event, suggesting that solar rotation over the two day separation period significantly decreased the chances of the in-situ shock encounter. We focus on the November 4 event because it propagates into a relatively undisturbed solar wind, and had a clearly associated ICME.

The SEP event time profile for the November 4, 1997 CME case, in the bottom panel of Fig. 1b, was remarkably simple considering the complicated appearance of the ICME signature. The following larger L1 shock and its SEP event from the November 6 CME could also have been simulated in the same CORHEL run, but the cone parameters derived for that later event were not well-determined. A general problem with sequential events such as this is that the coronagraph images for the second CME are often rendered unusable by the first event's SEPs affecting the imaging systems. Mason et al. (1999) discuss the November 1997 SEP events in some detail, estimating the time to maximum for the November 4 SEP event at ~8 h for 9 MeV/nucleon ions, compared to a 1.4 h direct propagation time to 1 AU. They estimated that the heliocentric distance of the primary injection of the SEPs from the shock in this case was ~23 Rs. They also point out that the spectral hardness of the second SEP event was greater,
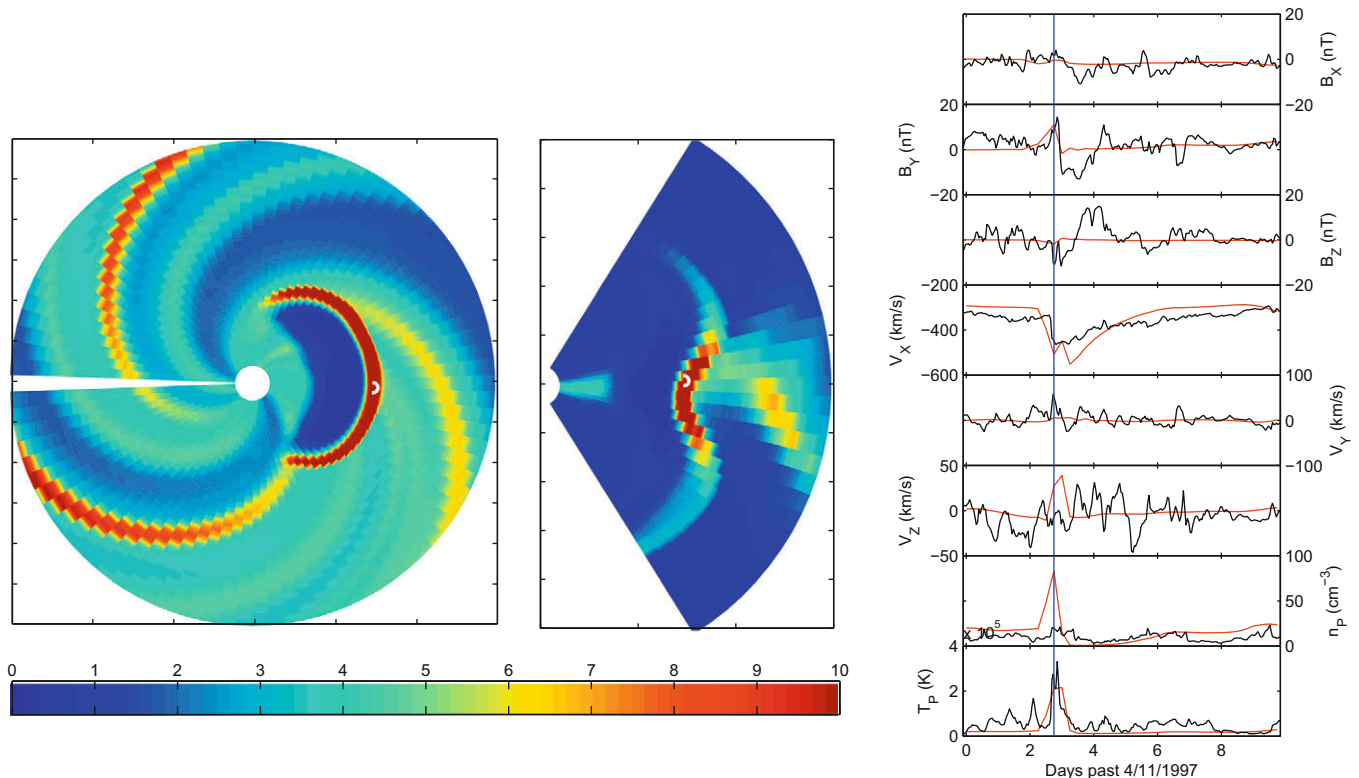

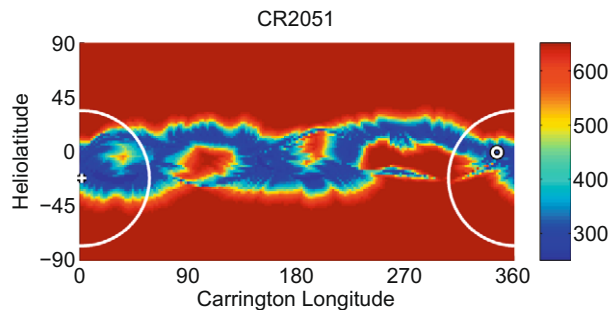Fig. 3b. Same as Fig. 2b but for the November 4, 1997 event CORHEL model.

Fig. 4a. Same as Fig. 2a but for the December 13, 2006 CME.

perhaps as a result of preacceleration of some particles by the earlier ICME's shock passage. One feature that distinguishes this event from the May SEP event is the relative lack of a proton flux depletion following the ESP signature. The arrival of the second event prompt fluxes almost coincident with the first event ESP feature may explain the lack of an effect of the November 4 CME ejecta in the observed time profile.

The cone model boundary conditions and interplanetary results for the November 4, 1997 CME case are shown in Fig. 3a and b, respectively. The cone model-based injection for this event, during Carrington Rotation 1929, was over 2X as broad and slightly faster than for the May 1997 event (see Table 1). While the comparison with the in-situ plasma and field observations is not as good as in the May 1997 case, it nevertheless represents one of the better cone model result comparisons as far as the time of arrival of the shock is concerned. As seen on the right of Fig. 3b, the observed

density compression is not well-matched by the simulation. However, we adopt this case as a test of how well the L1 shock jump must be reproduced to obtain a reasonable SEP event simulation. The rationale is that the calculated SEP event depends on the cumulative description of the modeled shock throughout its inner heliosphere transit, and not just at L1. This event's significantly wider disturbance than in the May 1997 case, as seen in the density contours in Fig. 3b, also predisposes the observer to a possibly longer shock connection time.

4.3. December 2006 event

The December 13, 2006 halo CME was observed after STEREO launch in October 2006, but before the STEREO imagers were commissioned, and before the spacecraft were in their heliocentric orbits. SOHO imagers captured this event and the closely spaced STEREO, ACE and Wind all detected essentially the same ICME starting December 15, seen in the OMNI data plot in Fig. 1c. This case represents the only major SEP event observed on STEREO before solar activity subsided into the cycle 23 minimum (von Rosenvinge et al., 2009). While we are not able to use these data as an example of a separated measurement of an ICME and SEP event, it nonetheless provides an interesting case for this modeling study.

The solar activity surrounding this event included four significant X-ray flares occurring in the associated active region as it passed over the visible disk between December 5 and December 14. In addition to the fast (~1800 km/s) 13
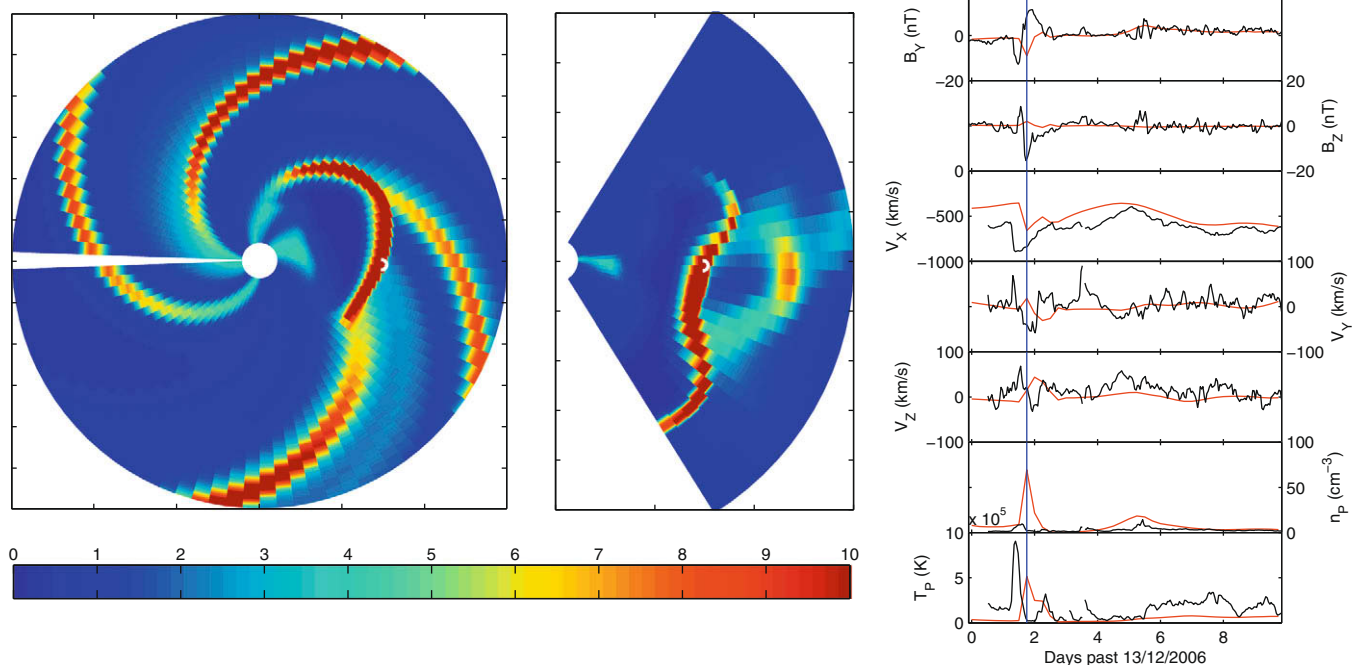

Fig. 4b. Same as Fig. 2b but for the December 13, 2006 event CORHEL model.

December halo CME, another halo CME with an estimated speed of ~1000 km/s occurred on December 14. Liu et al. (2008) describe further details of these eruptions and their solar signatures. The early flares (December 5, 6) occurred when the active region was on the eastern part of the disk, while the flares accompanying the December 13, 14 halo CMEs occurred at W23 and W46 longitudes, putting them in the sector where prompt SEPs are known to have the best magnetic connectivity to Earth. However, the presence of the eastern disk activity may be considered a factor in possible seed population production for later acceleration by the halo CME shocks. In fact the easternmost event on December 5 had the largest flare of the entire period.

The ICME disturbance(s) for this period (see Fig. 1c) have all the ideal characteristics of a classical ICME, including a leading shock, and a sheath or solar wind compression region followed by ejecta magnetic fields that slowly rotate as expected for a flux rope topology (Mulligan et al., 2008; Liu et al., 2008). The arrival time of the ejecta fields is consistent with their origin in the 13 December halo CME, but it is not clear whether any L1 plasma and field signature of the 14 December halo CME was detected, in part because of the ICME's simple appearance and in part because the observed ejecta magnetic fields can

be modeled as a single flux rope (Liu et al., 2008). It is thus possible that the L1 location was affected only by the 13 December event, a working assumption we adopt here.

As in the November 1997 case described above, the 13 December event was not isolated, but began near the end of a large eastern disk eruption a few days earlier, and overlapped the later 14 December event period while the ICME was passing L1 (e.g. Mulligan et al., 2008). Several detailed descriptions of the SEP measurements for this case, also seen at Ulysses at higher heliolatitudes, have been presented, in part because it provided a first on-orbit calibration for the STEREO energetic particle sensors (Mulligan et al., 2008; Malandraki et al., 2009; von Rosenvinge et al., 2009). The SEPs from the preceding eastern disk CME/ICME gradual event decay phase can still be seen at the time of the main event onset in the lower panel of Fig. 1c. In addition, multiple fluctuations in the SEP fluxes were detected during the ICME ejecta passage. It has been suggested these were caused by new injections from continued flaring in the same region (e.g. Mulligan et al., 2008), or by unusual anisotropies and complex magnetic connections to the shock source within the ejecta (von Rosenvinge et al., 2009). This case thus represents the most complicated case we subjected to the present modeling approach. Here we take the most simplistic view of the
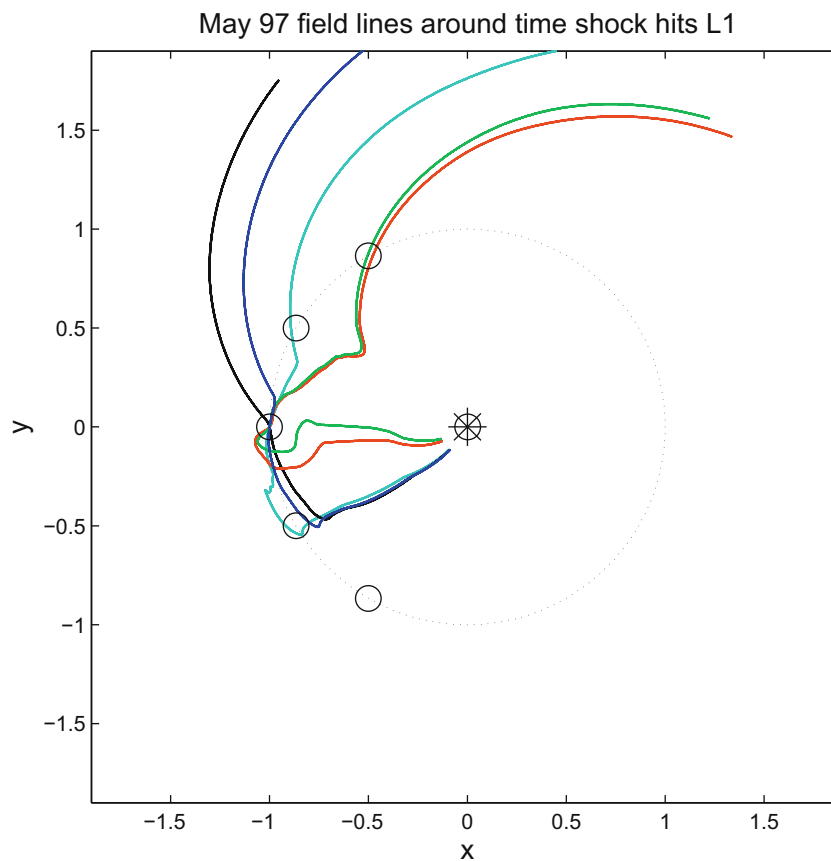

Fig. 5. A few snapshots of L1 observer-connected field lines from the May 1997 case, illustrating field line complexities in a structured interplanetary medium. The colors distinguish individual field lines. The small circles show the locations of five hypothetical 1 AU observers or two different STEREO separations at +/−30 and +/−60° from Earth, with the Earth in the center position

SEP event and presume, as for the ICME observations, that it is dominated by the 13 December CME-related shock source.

Fig. 4a and b shows the CORHEL inner boundary and 1 AU simulated L1 plasma and field time series for this case, which is the widest and fastest of the three cone model CMEs (see Table 1). The estimated speed of this event at 20 Rs was ~1200 km/s, indicating some deceleration in the corona relative to its initial speed. Note that the inner boundary velocity map for CR2051 (Fig. 4a) includes a more structured slow solar wind belt than in the two preceding cases. The comparison of the plasma and field data with the cone model results in Fig. 4b reinforces the idea that even the pre-shock conditions are more structured or may be unsteady. In this case the L1 shock jump may also be compromised by disturbed conditions from the flanks of the earlier eastern disk events, even though the cone model shock arrival timing is reasonable. In the future, this period may represent a good case for experimentation with multiple cone model CME injections. However for the present study we test the single event assumption for this case also.

5. Identifying and characterizing the CORHEL cone model shock

One of the primary challenges faced by the shock-accelerated SEP models is the proper identification and description of the interplanetary shock, and in particular, its location and evolving strength. This task is complicated by the limited spatial resolution of the MHD simulations, especially as heliocentric distance increases, coupled with potential confusion from other significant gradients that develop – including those from interactions of the high and low speed solar wind at low to mid-heliolatitudes. To routinely characterize the observer-connected shocks in the cone model results, we developed a shock-finding algorithm that searches for the largest gradients in the MHD parameters along an observer-connected field line at a particular time step. For this purpose, MHD grid snapshots are saved in CORHEL hdf format output files at ~6 min (event time) intervals, although a user can choose to alter this time resolution in their original CORHEL cone model run. Starting at the observer, a field line is traced in the grided data for each time step inward to the Sun, and outward to the CORHEL boundary at ~2 AU. The MHD variables at each position step along the field line are saved together with the position, in a file that reorders the data to trace continuously from the outermost point, inward. In the current version ~2500 field lines are saved for the equivalent number of time steps. Fig. 5 shows several field lines from a CORHEL run that illustrate the significant departure from a pure Parker Spiral geometry that occurs around the time of an event in the simulation. It is clear that the use of a Parker Spiral field description will fail to capture the complicated details of even a simple ICME disturbance such as that produced by a cone model CME.
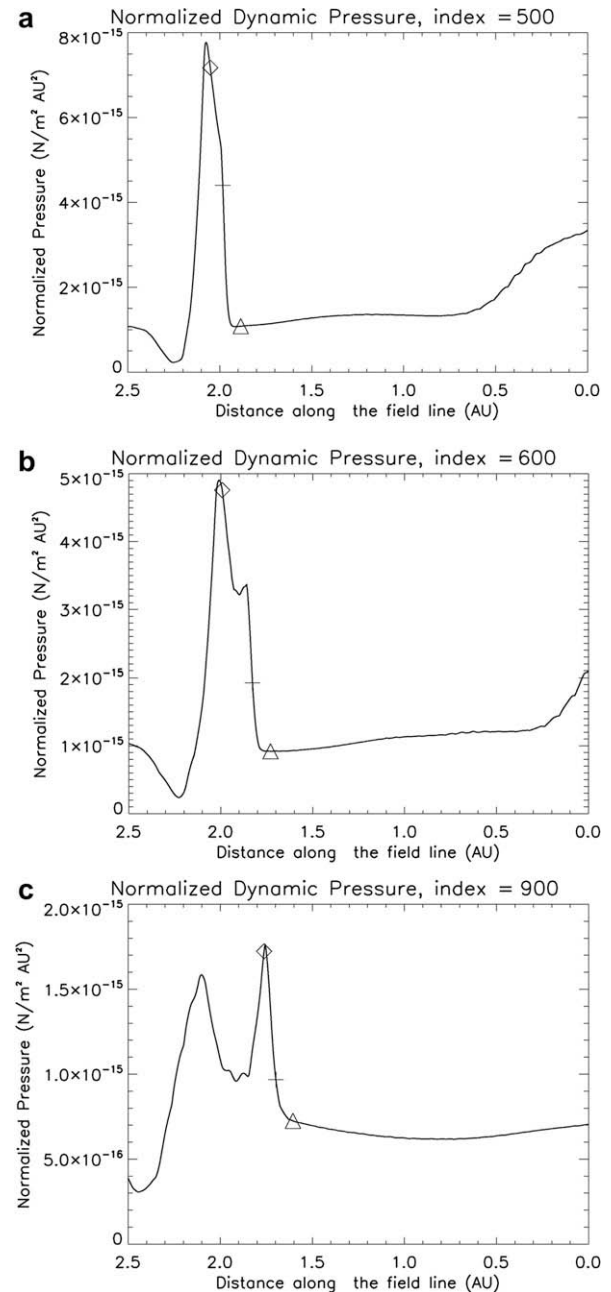
Fig. 6a-c. Three snapshots of shock finder results showing sample shock identifications (+) and jumps (bracketed by symbols) based on analysis of the dynamic pressure perturbations along observer-connected field lines in the CORHEL model. These illustrate the challenges faced by an automated search algorithm in the structured MHD simulation grid results. The CORHEL snapshot time steps of the frames are indicated in the panel titles, and occur in the order of increasing 'index': (a) 500, (b) 600, (c) 900. Here the inner boundary is on the left end of the distance axis so that the shock moves from left to right with time. The search for the shock starts at the 1 AU observer end of the field line (right end, or zero distance here) and moves toward the Sun (left). The quiet solar wind dynamic pressure gradient is removed by normalizing. The largest gradient along a field line that occurs within several grid points is identified as the shock (+). Determination of upstream (triangles) and downstream (diamonds) parameters used to calculate the shock compression ratios or jumps is described in the text. Downstream values are especially problematic because the sheath pileup in the disturbance is often difficult to distinguish from the shock ramp end point.

In the next computational step the gradients of the MHD variables are calculated along the field line and normalized by the square of the radial distance. A smoothing filter is then applied to the gradients to filter out numerical oscillations. The field line is searched for the largest filtered gradient in a specified MHD quantity, starting from the outermost point and moving inward. The location of the largest gradient is then identified as the shock location. From that point the gradients are followed inward until the filtered gradient changes sign. The location of the sign change, or ideally when the gradient is zero, is taken to be the downstream point. Then starting at the shock location the field line is traced outward until the MHD variable drops to less than 10% of its value at the shock location. This is taken to be the upstream point. If the shock was substantially structured by its interaction with the solar wind over modest scales, then an obliquely intersecting field line would not provide a very good sample of what is upstream and downstream. It could enter and leave the shock where conditions are quite different from a crossing along a local shock normal. However if the shock is relatively large scale and locally near-planar, at least over the span of the field line intersection, than the upstream and downstream parameters would be relatively uniform.

Given our use of MHD variables along field lines to compute the shock jump, this means the latter type of shock should produce a better match to our present shock jump calculation. In the present version of the code we accept any errors related to this approach to shock jump calculations, with the assumption that future improvements can occur.

Fig. 6a–c illustrate the normalized dynamic pressure along sampled field lines at different times, and the locations the algorithm identifies as the shock gradient start and stop (diamond and triangle symbols). We find that both dynamic pressure and density provide the clearest identification of shock gradients, with dynamic pressure the most robust. As described in Luhmann et al. (2007), the density compression ratio and other shock parameters are then calculated at the point of the largest gradient (+ symbols in Fig. 3a), and stored in a file containing the time history of the observer-connected shock location and strength. As suggested by the examples in Fig. 3a, upstream and downstream values used to calculate the jumps are difficult to determine. There is frequently little to no plateau in the downstream values, and the peak is identified as the downstream value, while the upstream may be either in the ambient medium or at some interim point if there is an inflection. When more than one shock or other large
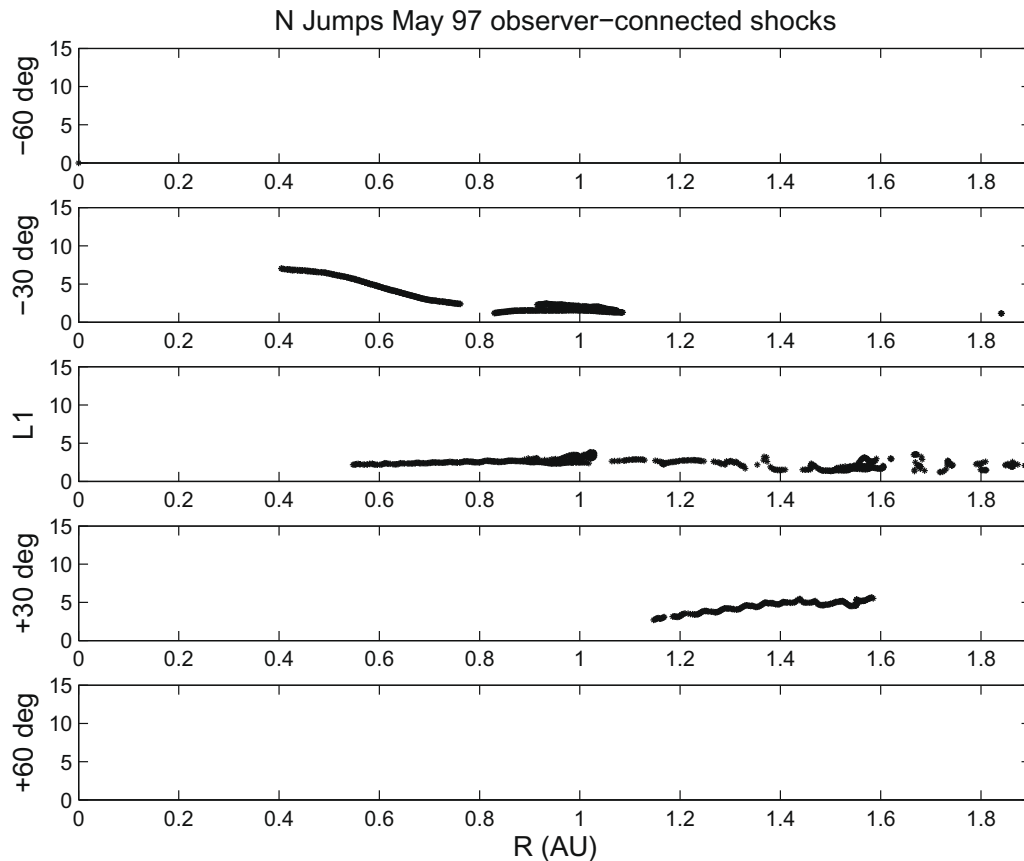

Fig. 7a. Observer-connected shock heliocentric locations and compression ratios or jumps found for the May 1997 event model at locations 60 and 30° trailing (−) L1, at L1, and at 30° and 60° leading (+) L1, from top to bottom. The jumps are defined in the standard way as the ratio of downstream and upstream values of density (*N*), as determined by the shock finder (see text). Jumps larger than the usual limit of 4 are found because the shock finding algorithm used often includes the following ICME sheath field pileup region in the evaluation of the downstream field (see text for further discussion of the challenges of identifying and characterizing the shock in the MHD heliospheric code results).
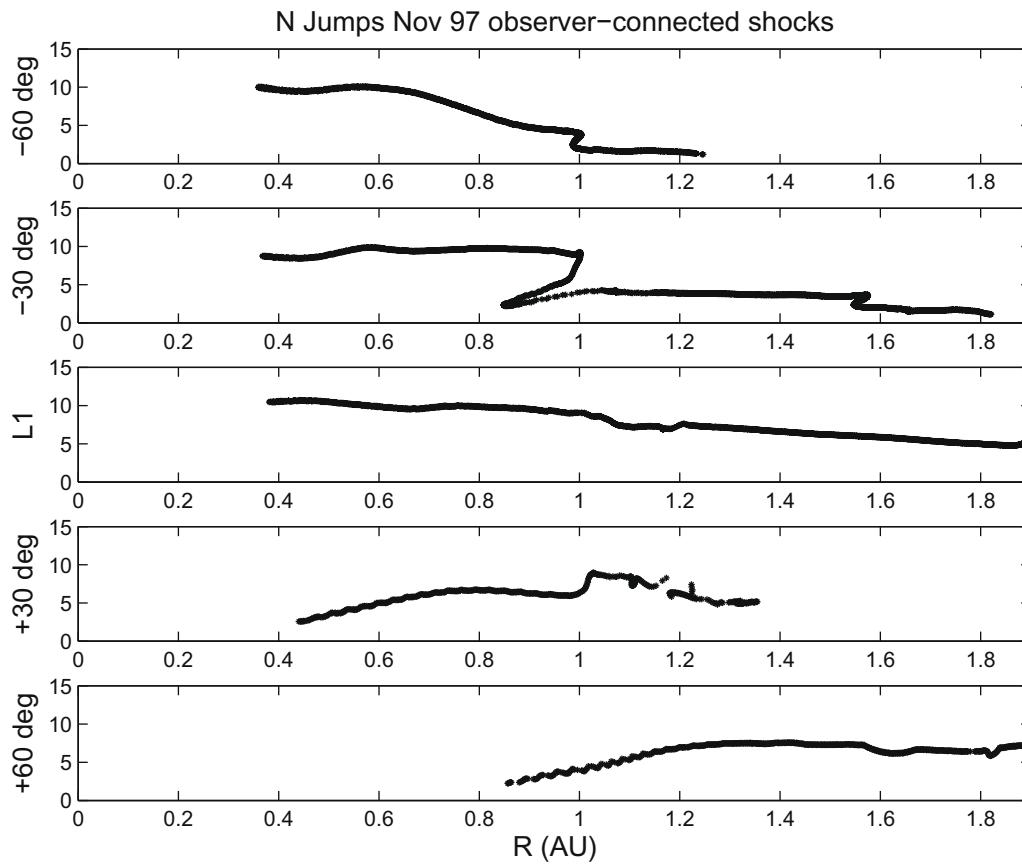
N Jumps Nov 97 observer−connected shocks

Fig. 7b. Same as Fig. 7a but for the November 1997 case. The large jumps are due to shock finder issues described in the text and in Fig. 5 caption.

gradient is present on a field line, the present shock finding algorithm saves information only for the strongest gradient. This means that if multiple CME injections have occurred, or if there is a stream interaction-related compression region present that produces a larger gradient than the cone model generated structure, that feature is automatically selected to describe the 'SEP' injection at that time step. Thus corotating shocks in ENLIL may also be sources of energetic particles in this treatment. We attempt to restrict the inclusion of the more distributed large gradients associated with stream interaction ridges by requiring that the identified largest gradient occupies less than 100 points along the field line (about a few tenths of an AU). One additional caveat is that use of the gradient along the field line can significantly underestimate the shock strength for quasiperpendicular shocks, but we assume for the present that the shock is so large-scale that the quasiparallel geometry describes the dominant source. This avoids the considerable complications of computing the jumps along the shock normal, with the final results providing the most straightforward test of this assumption.

Fig. 7a–c shows the shock strength histories obtained for each of the three events in this study, calculated for the five nominal observer locations in Fig. 5, representing the Earth (L1 point) and nominal STEREO spacecraft positions at 30° and 60° heliospheric longitude ahead (+, representing STEREO-A) and behind (−, representing

STEREO-B) the Earth's. It is important to understand that these histories are neither radial histories nor histories of the shock along a particular heliospheric field line. Rather they are the time sequence of shock strengths that affect these specific observers. The shock jump histories are quite complicated in some cases, and the value of the computed density compression, which we use to parameterize the SEP injections, often exceeds 4. As noted earlier, this depends on how a particular field line through the observer is configured and the surrounding structures. If there are stepped gradients, for example, the shock finder may select the part of the step that includes the compression maximum in the cone model material as the downstream rather than the shock ahead of it that is not well-separated from the entire sheath-like disturbance (e.g. as in Fig. 6b). The sample field lines plotted in Fig. 5 also illustrate the geometrical challenges of identifying upstream and downstream on a field line that undergoes many changes of direction as it is increasingly distorted by the ICME and the solar wind stream structure with which it interacts.

At this stage of development we work with the jumps in Figs. 7a–c and adjust the calibration factors for the injected SEP fluxes empirically, under the assumption that they still reflect the relative strength of the evolving shock source. In other words, when we set our fixed shock jump-dependent shock source description, we use a normalization factor that produces fluxes of the order of magnitude of the
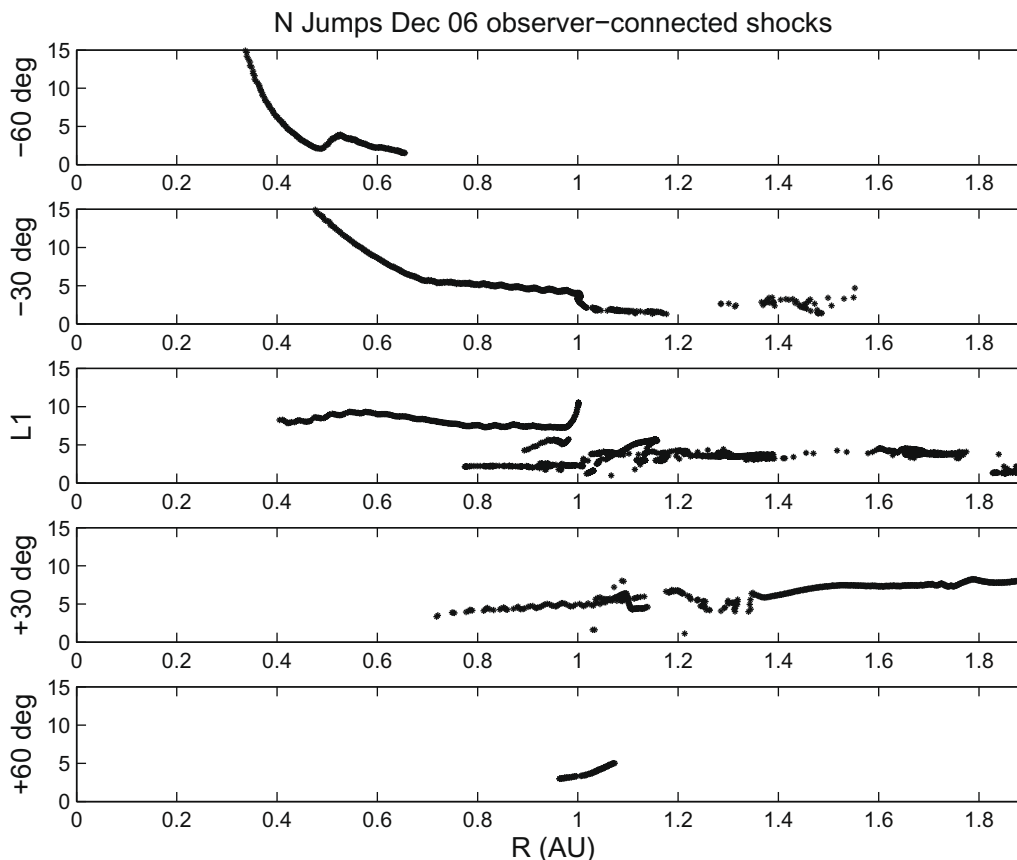
Fig. 7c. Same as Figs. 7a,b but for the December 2006 case. The relative noisiness of these results reflects the complicated structure of the interplanetary medium in this event, even under the simplified event assumptions.

observed fluxes. We accept that we are working with MHD model-derived jump conditions that reflect the general sense of the shock strength evolution, but are compromised in their values by mixing with the ICME sheath compression. Thus our source strength normalization, determined by roughly matching modeled to observed flux levels (with a single normalization factor for all events shown), implicitly takes this into account. It is nonetheless important that this normalization factor is the same for all events. We do not make event-by-event adjustments. We plan to eventually revise the shock finder program to use the shock normal direction to define the shock jump, however, this more desirable but more computationally intensive option will still be subject to the same difficulties of identifying what is upstream and what is downstream in a highly structured medium. We also expect the situation to be somewhat different when ejecta fields are introduced. Under such circumstances the shock may become better separated from its driver, and the ICME sheath region thus better defined. In any case shock identification in the MHD codes remains a key challenge for SEP event modeling.

6. Modeled SEP events

The modeled SEP event time series obtained using the shock histories described above are shown in Fig. 8a–c, which display differential fluxes at a range of energies between 1 and 100 MeV for the five observers. These results are intended to be illustrative of the capability of the approach, as they represent the same level of information a typical researcher or forecaster might have at their disposal. We tracked proton energies patterned on the IMP-8 detectors that provided exceptional observations for the May 12, 1997 event (Tylka, personal communication, 2004), though any energy can be specified in the model. Our use of the shock histories in Fig. 3b both illustrates an advantage of this model for considering a range of observer connection geometries, and gives an idea of the expected longitudinal differences in SEP event time profiles for 'STEREO' observers at 30° and 60° from L1 (see Fig. 5). The results are stacked with the farthest Earth-trailing location at the top, progressing through L1 down to the farthest Earth-leading location. Several features stand out in these results. One is that the longitudinal extent and strength of the shock (as inferred from Figs. 2–4 and Fig. 7a–c) determine the multipoint outcome, as expected. Another is that the details of the observer-connected shock structure seen in Fig. 7a–c are smoothed out in the SEP events by the integration of injections from the constantly moving and evolving shock source. Pitch angle distribution histories obtained from the SEP event model for each energy range show ~30–60° wide, field aligned beams that become nearly isotropic when the shock reaches the observer, and may
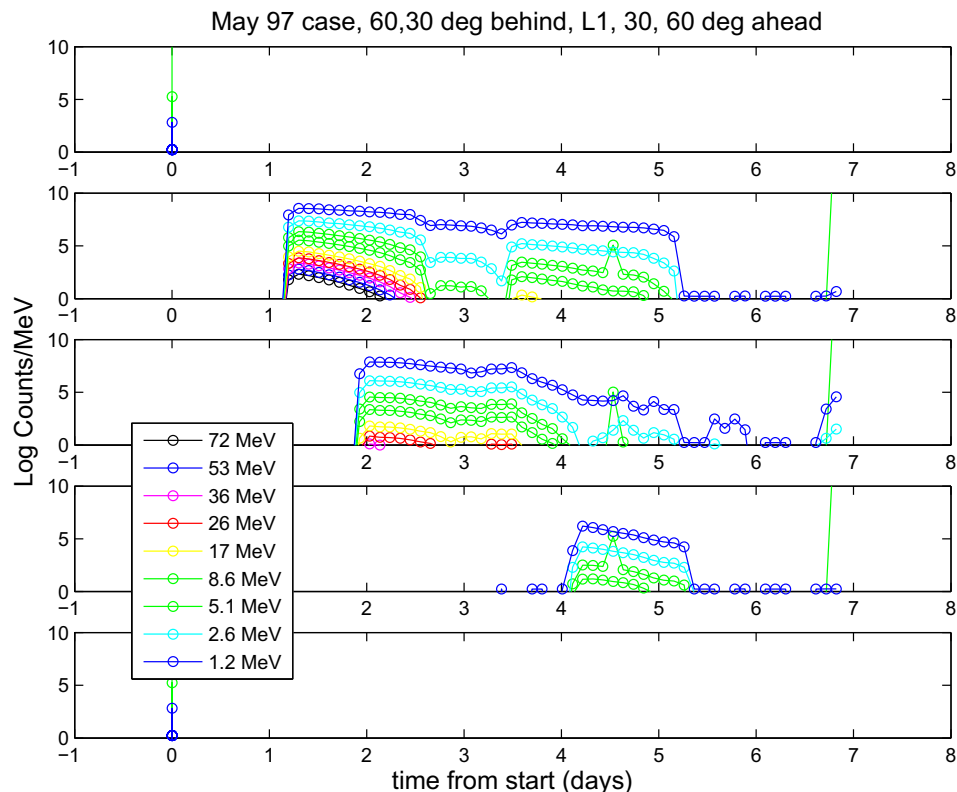
Fig. 8a. Results of the May 1997 SEP event modeling for the five observer locations in Fig. 5, with the 60° Earth trailing location at the top. These are nominal differential fluxes at the energies shown in the legend, similar to IMP-8 detector channels. The flux scales reflect nominal model results not normalized to physical values. The outlying 'spikes' represent a few of the injected particles that follow atypical paths due to either numerical errors in interpolating the MHD fields on the grid or to a particularly unusual sampling of the MHD simulation fields. They are retained to illustrate the true appearance of the model results, but should not be regarded as the most reliable points in the time profiles.

appear bidirectional afterward. Analyses of these anisotropies, which are not generally available in historical event data, will be discussed in a future report. However, due to the effect of the magnetic mirror force in the diverging interplanetary field, early SEP event field-aligned distributions are expected when the observer is connected to the shock source closer to the Sun (e.g. Reames et al., 2001).

The May 12, 1997 case in Fig. 8a shows significant differences in both fluxes and time profiles from observer to observer. As this is the narrowest halo CME (see Table 1, Fig. 2b), only the most centrally located observers detect the ICME shock-associated SEPs. The trailing observer at –30 degrees longitude separation sees the highest SEP fluxes and most energetic spectra. Their event also lasts the longest time, consistent with the length of the different shock connection histories in Fig. 7a. In Fig. 8b, the November 1997 case, resulting from a much wider CME (Table 1), is seen to produce nearly identical SEP time profiles for the Earth-trailing and L1 observers. The modeled event onset is delayed the most at the leading observer's position, where only the flank of the shock (see Fig. 3b) is intercepted by the observer field line after the shock nose is well-past the centrally located observer. The spectrum is also softest or least energetic at this location, commensurate with the weaker shock at the flank (see Fig. 7b). The results for the December 2006 case, in Fig. 7c, exhibit more

variation from location to location, and more structure in the time profiles. In this case there is less centrally located symmetry in the shock development (Fig. 4b), and a more structured background slow solar wind belt with which it interacts (Fig. 4a). Again the leading observer experiences the weakest, least energetic, and shortest duration modeled SEP event due to its glancing shock connection (Fig. 7c). The L1 location experiences the longest lasting event, but the closer trailing observer experiences the largest fluxes and hardest spectra around the event onset, in both the November 1997 and December 2006 cases the trailing and L1 observer profiles show the most closely coincident onsets. This is because the upstream field connections to the simulated shock front occur earliest at these locations, when the halo CME shock is close to the Sun.

In Fig. 9a–c the modeled L1 results have been calculated for energies better suited to approximate the integral fluxes in the OMNI data (Fig. 1a–c), and normalized (with a common factor for all three events) to the observed values for comparison. Once the best single normalization factor was determined from visual comparisons to all of the time series, no adjustments were made from event to event or observer to observer. This normalization factor applied to the entire time profile and is determined by numerical rather than physical considerations, most specifically on the number of test particles injected at each time step of
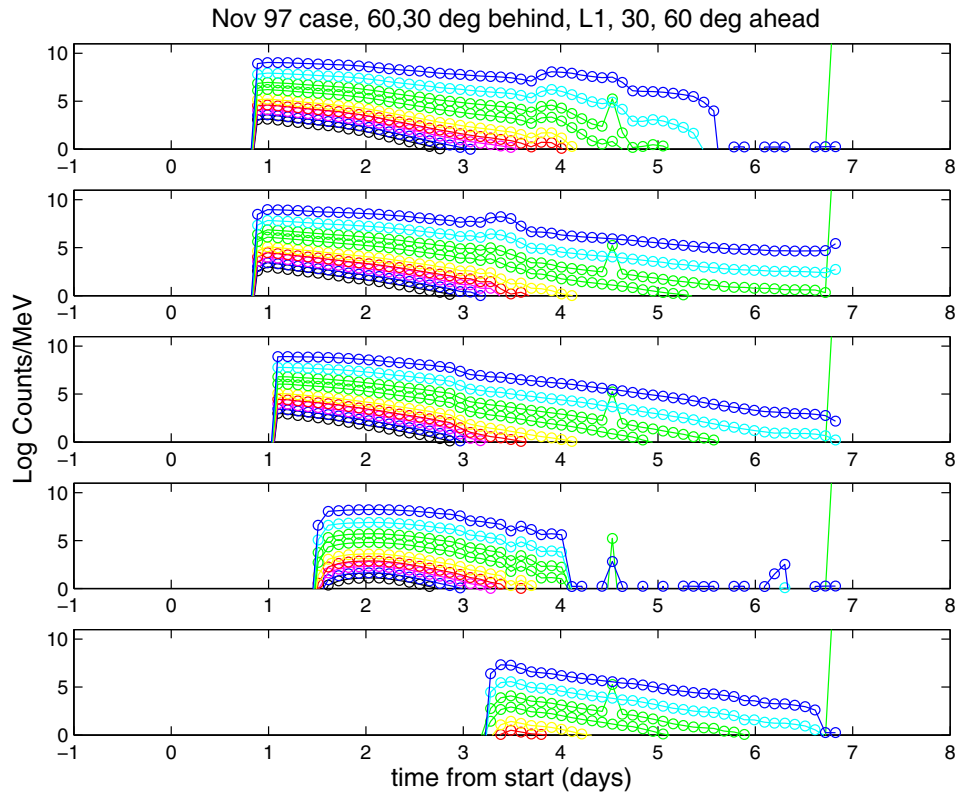
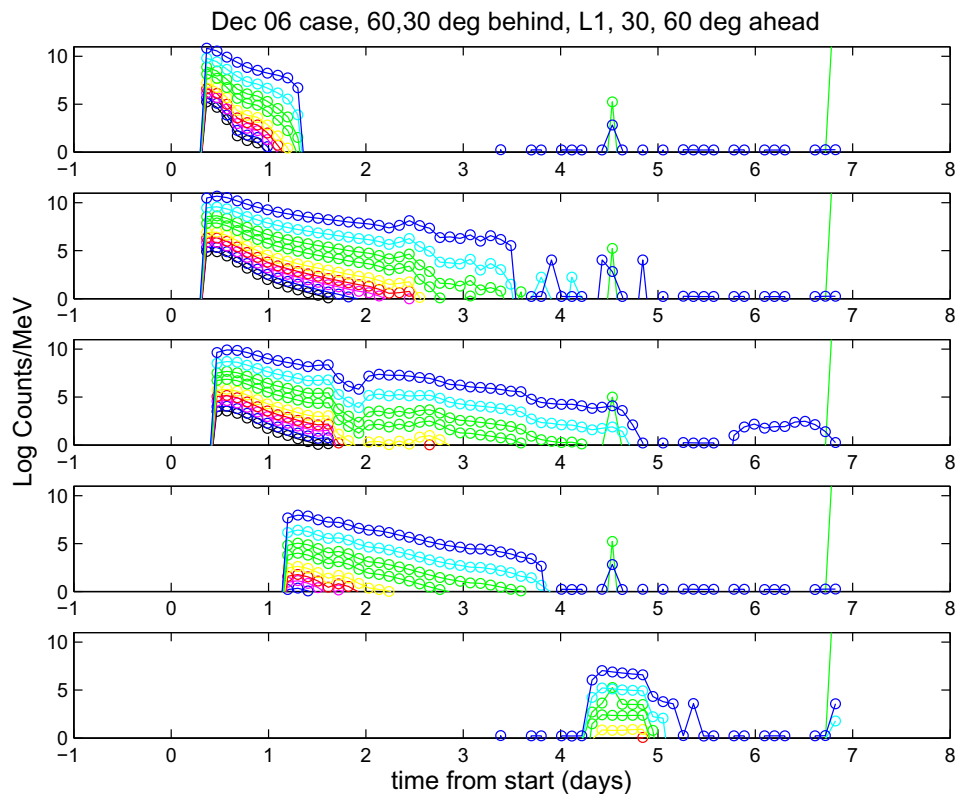Fig. 8b. Same as Fig. 6a but for the November 1997 case.

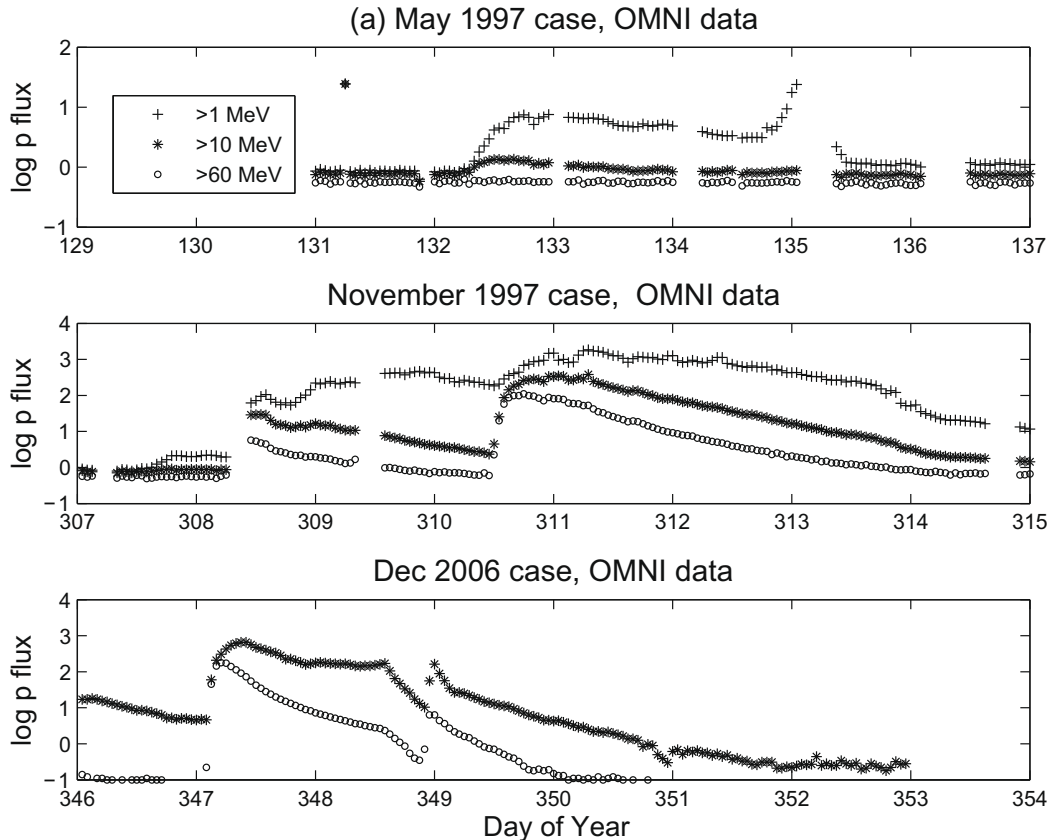Fig. 8c. Same as Fig. 6a but for the December 2006 case.

Fig. 9. Comparison of OMNI observations ((a), above) with model results ((b), next page), where the model results now approximate integral fluxes at the IMP-8 energies (see Fig. 8a for color code and energies) and the model flux scale has been approximately normalized to the data. The November 1997 model event in the right center panel does not include the second injection seen in its OMNI counterpart at left.

the SEP event model code (see Luhmann et al., 2007 for a background discussion). The model calculations assume the relative SEP production efficiency in these examples depends only on the connected shock strengths indicated in Fig. 6a-c. Such fixed normalization must be an attribute of any scheme that would be useful for SEP event forecasting. The modeled L1 time series in Figs. 9a–c are roughly consistent with the observations in spite of the many approximations and simplifications made. Both the integral flux levels and profile shapes are qualitatively similar, although the modeled time profiles appear to have an overall shorter duration than the observed profiles. This could be due to the details of the modeled ICME, which determines the shape and spatial extent of the shock using the cone model initiation, and is not necessarily a deficiency of the SEP event calculation. The December 2006 case is especially notable because the model seems to capture some of the structure in the time profile. While it has been previously suggested (e.g. Mulligan et al., 2008) that this structure may result from a second injection of particles, our results indicate that an alternative interpretation may lie the history of the observer-shock connections, which are not always simple, nor is the shock structure itself (e.g. von Rosenvinge et al., 2009). The cone model-initiated ICMEs for these events, which include the ambient solar wind structure, have the potential to capture some of this detailed geometry.

One of the commonly observed SEP event features that we do not capture with the current modeling scheme is the sometimes notably gradual onset of eastern disk CME-related events (Cane et al., 1988). In this study of L1 halo CME cases, the calculated time profiles for Earth-leading, or STEREO A positions for narrower events such as May 1997 (Fig. 8a) show onsets similar to the L1 profiles. It is not clear at this stage whether this is a consequence of the cone model initiation (which omits portions of the initial shock radial profile and has sharp boundaries at the cone edges), of our shock search criteria that may bias against weak and/or highly perpendicular ICME shocks, the lack of a shock normal angle dependence in our shock source description, or the lack of cross-field transport in our current transport model. Further numerical experimentation is necessary to understand this model behavior.

7. Conclusions

In this paper we have described some initial tests of a gradual SEP proton event model-based on cone model-initiated ICMEs within a realistic solar wind model. The approach we use emphasizes the non-diffusive aspects of SEP events outside of a localized shock source 'black box'. It is a completely forward-modeling approach that uses observations only to characterize the boundary conditions and CME-
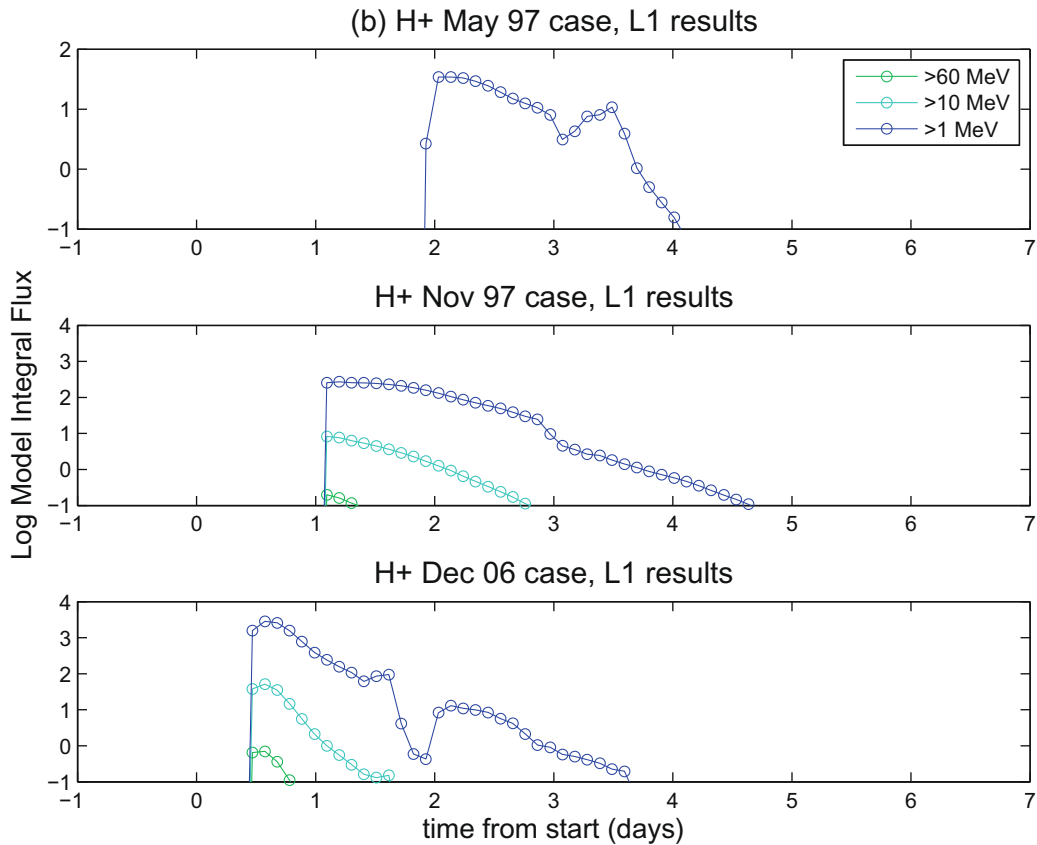
Fig. 9 (*continued*)

related disturbance near the Sun. We calculated SEP event flux time profiles for three Halo CME events observed by spacecraft at five 1 AU observer locations including L1, where observations were generally available. The results are determined by the underlying shock evolution and the magnetic field connections to the observer. We found some correspondences between the model results and L1 in-situ measurements, although the multipoint aspects of the model event predictions could not be tested, pending further observations from STEREO. The need for good CME/ICME simulations to provide accurate background information for realistic SEP event models is clear from these results, regardless of the need (or not) for scattering parameterizations during SEP transport.

The aim of this study was to provide further tests of what may lead to a useful SEP event analysis and forecast tool when coupled with coronagraph observations. If the cone model of CMEs used to initiate interplanetary disturbances continues to be the most practical approach to real ICME prediction and simulation, the framework applied here may represent an early step to a SEP event model that is potentially general. Future efforts will involve experimentation with different types of events, including real multipoint cases, with adjusted assumptions regarding the shock identification and source characterization, with particle transport optionally modified by scattering processes, and with CME/ICME MHD model case studies that

include the corona and simulated ejecta magnetic fields. Other features such as the ESP portion of the event require further study and developments.

References

Aran, A., Sanahuja, B., Lario, D. SOLPENCO: a solar particle engineering code. Adv. Space Res. 37, 1240–1246, 2006.

Aran, A., Lario, D., Sanahuja, B., Marsden, R.G., Dryer, M., Fry, C.D., McKenna-Lawlor, S.M.P. Modeling and forecasting solar energetic particle events at Mars: the event on 6 March 1989. Astron. Astrophys. 469, 1123–1134, 2007.

Aran, A., Sanahuja, B., Lario, D. Comparing proton fluxes of central meridian SEP events with those predicted by SOLPENCO. Adv. Space Res. 42, 1492–1499, 2008.

Arge, C.N., Luhmann, J.G., Odstrcil, D., Schrijver, C.J., Li, Y. Stream structure and coronal sources of the solar wind during the May 12, 1997 CME. J. Atmos. Solar Terr. Phys. 66, 1295–1309, 2004.

Balch, C.C. SEC proton prediction model: verification and analysis. Radiat. Meas. 30, 231, 1999.

Cane, H.V. Coronal mass ejections and Forbush decreases. Space Sci. Rev. 93, 55–77, 2000.

Cane, H.V., Reames, D.V., Rosenvinge, T.T. The role of interplanetary shocks in the longitude distribution of solar energetic particles. J. Geophys. Res. 93, 9555, 1988.

Cane, H.V., von Rosenvinge, T.T., Cohen, C.M.S., Mewaldt, R.A. Two components in major solar particle events. Geophys. Res. Lett. 30, 2002GL016580, 2003.

Case, A.W., Spence, H.E., Owens, M.J., Riley, P., Odstrcil, D. Ambient solar winds effect on ICME transit times. Geophys. Res. Lett. 35, doi:10.1029/2008GL034493, 2008.

Dryer, M. MHD simulations of solar and interplanetary phenomena. Astrophys. Space Sci. 243, 133, 1996.

Eto, S. et al. Relation between Moreton wave and EIT wave observed on 1997 November 4. PASJ 54, 481–491, 2002.

Fisher, R.R., Munro, R.H. Coronal transient geometry I – The flare associated event of 1981 March 25. Astrophys. J. 280, 428–439, 1984.

Fry, C.G., Dryer, M., Smith, Z., Sun, W., Deehr, C.S., Akasofu, S.-I. Forecasting solar wind structures and shock arrival times using an ensemble of models. J. Geophys. Res. 108, doi:10.1029/2002JA009474, 2003.

Giacalone, J., Kota, J. Acceleration of solar energetic particles by shocks. Space Sci. Rev. 124, 277–288, 2006.

Heras, A.M., Sanahuja, B., Smith, Z.K., Detman, T., Dryer, M. The influence of the large-scale interplanetary shock structure on a low energy particle event. Astrophys. J. 391, 359–369, 1992.

Heras, A.M., Sanahuja, B., Sanderson, T.R., Marsden, R.G., Wenzel, K.P. Observational signatures of the influence of the interplanetary shocks on the associated low-energy particle events. J. Geophys. Res. 99, 43–51, 1994.

Howard, R.A., Michels, D.J., Sheeley Jr., N.R., Koomen, M.J. The observation of a coronal transient directed at Earth. ApJ 263, L101, 1982.

Jones, F.C., Ellison, D.C. The plasma physics of shock acceleration. Space Sci. Rev. 58, 259–346, 1991.

Kahler, S.W. Solar sources of heliospheric energetic electron events – Shocks or flares? Space Sci. Rev. 129, 359–390, 2007.

Kallenrode, M.-B., Wibberenz, G. Propagation of particles injected from interplanetary shocks: black box model and its consequences for acceleration theory and data interpretation. J. Geophys. Res. 102, 22311–22334, 1997.

King, J.H., Papitashvilii, N.E. Interplanetary Medium Data Book, Suppl. 5, 1988–1993, NSSDC WDCA-R&S 94-08 NASA NSSDC/GSFC, Greenbelt, MD, 1994.

Klecker, B., Kunow, H., Cane, H.V., Dalla, S., Heber, B., Kecstkemety, K., Klein, K.L., Kota, J., Kucharek, H., Lario, D., Lee, M.A., Popecki, M., Posner, A., Rodriguez-Pacheco, J., Sanderson, T., Simnett, G.M., Roelof, E.C. Energetic particle observations. Space Sci. Rev. 123, 217–250, 2006.

Kocharov, L., Pizzo, V.J., Odstrcil, D., Zwickl, R.D. A unified model of solar energetic particle transport in structured solar wind. J. Geophys. Res. 114, 10.029/2008JA013837, 2009.

Kota, J., Manchester, W.B., Jokipii, J.R., DeZeeuw, D.L., Gombosi, T.I. Simulations of SEP acceleration and transport at CME-driven shocks, in: The Physics of Collision less Shocks, AIP Conf. Proc., vol. 781, pp. 201–206, 2005.

Lario, D., Sanahua, B., Heras, A.M. Modeling the interplanetary propagation of 0.1–20 MeV shock accelerated protons II: energy spectrum and evolution of the injection rate. Adv. Space Res. 20, 121–126, 1997.

Lario, D., Sanahuja, B., Heras, A.M. Energetic particle events: efficiency of interplanetary shocks as $50\,keV < E < 100\,MeV$ proton accelerators. ApJ 509, 415, 1998.

Lee, M.A. Coupled hydromagnetic wave excitation and ion acceleration at interplanetary traveling shocks. J. Geophys. Res. 88, 6109–6119, 1983.

Lee, M.A. Coupled hydromagnetic wave excitation and ion acceleration at an evolving coronal/interplanetary shock. Astrophys. J. Suppl. 158, 38–67, 2005.

Lee, C.O., Luhmann, J.G., Odstrcil, D., MacNeice, P.J., de Pater, I., Riley, P., Arge, C.N. The solar wind at 1 AU during the declining phase of solar cycle 23: comparison of 3D numerical model results with observations. Sol. Phys. 254, 155–183, 2009.

Gang, Li, Zank, G.P., Rice, W.K.M. Energetic particle acceleration and transport at coronal mass ejection-driven shocks. J. Geophys. Res. 108, 2002JA009666, 2003.

Liu, Y. Photospheric magnetic field observations during the May 12, 1997 CME and their implications for modeling that event. J. Atmos. Solar Terr. Phys. 66, 1283–1294, 2004.

Liu, Y., Luhmann, J.G., Mueller-Mellin, R., Schroeder, P.C., Wang, L., Lin, R.P., Bale, S.D., Li, Y., Acuna, M.H., Sauvaud, J-A. A comprehensive view of the 2006 December 13 CME: from the Sun to interplanetary space. Astrophys. J. 689, 563–571, 2008.

Luhmann, J.G., Solomon, S.C., Linker, J.A., Lyon, J.G., Mikic, Z., Odstrcil, D., Wang, W., Wiltberger, M. Coupled model simulation of a Sun-to-Earth space weather event. J. Atmos. Solar Terr. Phys. 66 (15-16), 1243–1256, 2004.

Luhmann, J.G., Ledvina, S.A., Krauss-Varban, D., Odstrcil, D., Riley, P. A heliospheric simulation-based approach to SEP source and transport modeling. Adv. Space Res. 40 (3), 295–303, 2007.

Malandraki, O.E., Marsden, R.G., Lario, D., Tranquille, C., Heber, B., Mewaldt, R.A., Cohen, C.M.S., Lanzerotti, L.J., Forsyth, R.J., Elliott, H.A., Vogiatzis, I.I., Geranios, A. Energetic particle observations and propagation in the three-dimensional heliosphere during the 2006 December events. ApJ 704, 469–476, 2009.

Mason, G.M., Cohen, C.M.S., Cummings, A.C., et al. Particle acceleration and sources in the November 1997 solar energetic particle events. Geophys. Res. Lett. 26, 141–144, 1999.

Mewaldt, R.A. Solar energetic particle composition, spectra, and space weather. Space Sci. Rev. 124, 303–316, 2006.

Mulligan, T., Russell, C.T., Anderson, B.J., Lohr, D.A., Rust, D., Toth, B.A., Zanetti, L.J., Acuna, M.H., Lepping, R.P., Gosling, J.T. Intercomparison of NEAR and wind interplanetary corona mass ejection observations. J. Geophys. Res. 104, 28217–28223, 1999.

Mulligan, T., Blake, J.B., Mewaldt, R.A. Unusual solar energetic proton fluxes at 1 AU within an interplanetary CME, in: Proc. ICRC, 30th International Cosmic Ray Conference, Merida, Mexico, AIP, pp. 179–182, 2008.

Ng, C.K., Reames, D.V. Focused interplanetary transport of approximately 1 MeV solar energetic protons through self-generated Alfven waves. ApJ 424, 1032–1048, 1994.

Ng, C.K., Reames, D.V., Tylka, A.J. Effect of proton-amplified waves on the evolution of solar energetic particle composition in gradual events. Geophys. Res. Lett. 26, 2145–2148, 1999.

Odstrcil, D., Pizzo, V.J. Distortion of the interplanetary magnetic field by three dimensional propagation of coronal mass ejections in a structures solar wind. J. Geophys. Res. 104, 28225–28239, 1999.

Odstrcil, D., Riley, P., Zhao, X.P. Numerical simulation of the 12 May 1997 interplanetary event. J. Geophys. Res. 109, 2003JA010135, 2004.

Odstrcil, D., Pizzo, V.J., Arge, C.N. Propagation of the 12 May 1997 interplanetary coronal mass ejection in evolving solar wind structures. J. Geophys. Res. 110, 2004JA010745, 2005.

Owens, M.J., Spence, H.E., McGregor, S., Hughes, W.J., Quinn, J.M., Arge, C.N., Riley, P., Linker, J., Odstrcil, D. Metrics for solar wind prediction models: comparison of empirical, hybrid and physics-based schemes with 8 years of L1 observations. Space Weather J. 6, doi:10.1029/2007SW000380, 2008.

Pei, C., Jokipii, J.R., Giacalone, J. Effect of a random magnetic field on the onset times of solar particle events. Astrophys. J. 641, 1222–1226, 2006.

Plunkett, S.P., Thompson, B.J., Howard, R.A., Michels, D.J., St. Cyr, O.C., Tappin, S.J., Schwenn, R., Lamy, P.L. LASCO observations of an Earth-directed coronal mass ejection on May 12, 1997. Geophys. Res. Lett. 25, 2477–2480, 1998.

Reames, D.V. Particle acceleration at the Sun and in the Heliosphere. Space Sci. Rev. 90, 413, 1999.

Reames, D.V., Ng, C.K., Berdichevsky, D. Angular distributions of solar energetic particles. ApJ 550, 1064–1074, 2001.

Riley, P., Gosling, J.T., Pizzo, V.J. A two-dimensional simulation of the radial and latitudinal evolution of a solar wind disturbance driven by a fast, high pressure coronal mass ejection. J. Geophys. Res. 102, 14677–14686, 1997.

Riley, P., Linker, J.A., Mikic, Z. An empirically-driven global MHD model of the solar corona and inner heliosphere. J. Geophys. Res. 106, 15889, 2001.

Ruffolo, D., Khumlumlert, T., Youngdee, W. Deconvolution of interplanetary transport of solar energetic particles. J. Geophys. Res. 103, 20591–20602, 1998.

Scholer, M., Morfill, G.E. Simulation of solar flare particle interaction with interplanetary shock waves. Sol. Phys. 45, 227–240, 1975.

Smith, Z.K., Dryer, M., Lawlor, S.M.P., Fry, C.D., Deehr, C.S., Sun, W. Operational validation of HAFv2's predictions of interplanetary shock arrivals at Earth: declining phase of solar cycle 23. J. Geophys. Res. 114, 10.029/2008JA013836, 2009.

Taktakishvili, A., Kuznetsova, M., MacNeice, P., Hesse, M., Rastaetter, L., Pulkkinenen, A., Chulaki, A., Odstrcil, D. Validation of the coronal mass ejection predictions at the Earth orbit estimated by ENLIL heliospheric cone model. Space Weather 7, doi:10.1029/2008SW000448, 2009.

Thompson, B.J., Plunkett, S.P., Gurman, J.B., Newmark, J.S., St. Cyr, O.C., Michels, D.J. SOHO/EIT observations of an Earth-directed coronal mass ejection on May 12, 1997. Geophys. Res. Lett. 25, 2465–2468, 1998.

Tylka, A.J. New insights on solar energetic particles from wind and ACE. J. Geophys. Res. 106, 25333–25352, 2001.

Tylka, A.J., Lee, M.A. A model for spectral and compositional variability at high energies in large, gradual solar particle events. Astrophys. J. 646, 1319–1334, 2006.

von Rosenvinge, T., Richardson, I., Reames, D., Cohen, C., Cummings, A., Leske, R., Mewaldt, R., Stone, E.C., Wiedenbeck, M. The solar energetic particle event of December 14, 2006. Solar Phys. s256, 443–462, 2009.

Webb, D.F., Lepping, R.P., Burlaga, L.F., DeForest, C.E., Larson, D.E., Martin, S.F., Plunkett, S.P., Rust, D.M. The origin and development of the May 1997 magnetic cloud. J. Geophys. Res. 105, 27251–27260, 2000.

Zhao, X-P., Plunkett, S.P., Liu, W. Determination of geometrical and kinematical properties of halo coronal mass ejections using the cone model. J. Geophys. Res. 107, 1223, 2002.